Title
Targeting CD46 for both adenocarcinoma and neuroendocrine prostate cancer.

Journal
JCI insight, 3(17)

ISSN
2379-3708

Authors
Su, Yang
Liu, Yue
Behrens, Christopher R
et al.

Publication Date
2018-09-01

DOI
10.1172/jci.insight.121497

Peer reviewed

JCI insight

RESEARCH ARTICLE

Targeting CD46 for both adenocarcinoma and neuroendocrine prostate cancer

Yang Su,[1] Yue Liu,[1] Christopher R. Behrens,[1] Scott Bidlingmaier,[1] Nam-Kyung Lee,[1] Rahul Aggarwal,[2,3] Daniel W. Sherbenou,[2] Alma L. Burlingame,[4] Byron C. Hann,[3] Jeffry P. Simko,[3,5] Gayatri Premasekharan,[3,6] Pamela L. Paris,[3,6] Marc A. Shuman,[2,6] Youngho Seo,[7] Eric J. Small,[2,3,6] and Bin Liu[1,3]

[1]Department of Anesthesia, [2]Department of Medicine, [3]Helen Diller Family Comprehensive Cancer Center, [4]Department of Pharmaceutical Chemistry, [5]Department of Pathology, [6]Department of Urology, and [7]Department of Radiology and Biomedical Imaging, UCSF, San Francisco, California, USA.

Although initially responsive to androgen signaling inhibitors (ASIs), metastatic castration-resistant prostate cancer (mCRPC) inevitably develops and is incurable. In addition to adenocarcinoma (adeno), neuroendocrine prostate cancer (NEPC) emerges to confer ASI resistance. We have previously combined laser capture microdissection and phage antibody display library selection on human cancer specimens and identified novel internalizing antibodies binding to tumor cells residing in their tissue microenvironment. We identified the target antigen for one of these antibodies as CD46, a multifunctional protein that is best known for negatively regulating the innate immune system. CD46 is overexpressed in primary tumor tissue and CRPC (localized and metastatic; adeno and NEPC), but expressed at low levels on normal tissues except for placental trophoblasts and prostate epithelium. Abiraterone- and enzalutamide-treated mCRPC cells upregulate cell surface CD46 expression. Genomic analysis showed that the CD46 gene is gained in 45% abiraterone-resistant mCRPC patients. We conjugated a tubulin inhibitor to our macropinocytosing anti-CD46 antibody and showed that the resulting antibody-drug conjugate (ADC) potently and selectively kills both adeno and NEPC cell lines in vitro (sub-nM EC_{50}) but not normal cells. CD46 ADC regressed and eliminated an mCRPC cell line xenograft in vivo in both subcutaneous and intrafemoral models. Exploratory toxicology studies of the CD46 ADC in non-human primates demonstrated an acceptable safety profile. Thus, CD46 is an excellent target for antibody-based therapy development, which has potential to be applicable to both adenocarcinoma and neuroendocrine types of mCRPC that are resistant to current treatment.

Introduction

The widespread application of the androgen signaling inhibitors (ASIs) abiraterone and enzalutamide has significantly improved outcomes for men with metastatic castration-resistant prostate cancer (mCRPC) (1–4). However, development of resistance to these agents is universal, and sequential targeting of the androgen receptor (AR) signaling axis has met with limited clinical success (5, 6). The phenotype that emerges at the time of ASI resistance is frequently characterized by an aggressive phenotype, with development of neuroendocrine prostate cancer (NEPC) (7, 8). In this setting, there is an urgent need for novel therapies to improve outcomes.

Primary tumors often retain cell surface antigens expressed in the normal tissue from which the tumors are derived. Some of these tumor-associated cell surface antigens have a restricted overall normal tissue expression pattern and may be suitable for the development of antibody-based targeted therapies (9–15). However, if these antigens are not required for tumor survival, they may be lost during disease progression and heterogeneously expressed in late-stage cancers (16–18). To develop effective therapy, it is desirable to target antigens that perform functions critical for tumor growth and survival in an immunocompetent host and are homogenously expressed by advanced tumors. In addition, internalization is desired for therapies that require intracellular payload delivery (19–23). Finally, it is important to differentiate true tumor antigens that are expressed by tumor cells in their natural microenvironment as opposed to cell line artifacts incurred during prolonged in vitro culture (24, 25).

Authorship note: YS, YL, CRB, and SB contributed equally to this work.

Conflict of interest: BL is a founder and equity holder of Fortis Therapeutics Inc., which licensed intellectual properties from the University of California and is taking the anti-CD46 antibody–drug conjugate to clinical trials. EJS is an advisor and equity holder of Fortis Therapeutics Inc. BL, MAS, and Y. Seo hold equity shares in Molecular Imaging and Therapeutics Inc., which were converted to equity shares in Fortis Therapeutics Inc.

Submitted: May 3, 2018
Accepted: July 24, 2018
Published: September 6, 2018

Reference information:
JCI Insight. 2018;3(17):e121497.
https://doi.org/10.1172/jci.insight.121497.

We have previously developed a laser capture microdissection–based (LCM-based) strategy that enables selection of novel internalizing phage antibody against tumor cells in situ residing in their natural stromal microenvironment (24). We identified a panel of single-chain variable domain fragments (scFvs) that possess desired properties for antibody therapy development (24): (i) binding to live tumor cell lines, including mCRPC lines; (ii) binding to prostate tumor cells in situ; (iii) binding to rapidly internalizing epitopes. We went on to show by single-photon emission computed tomography that one of the scFvs, UA20, rapidly accumulates at tumor sites in vivo with an uptake ratio of tumor to neighboring non-tumor tissue of greater than 70:1 (26).

We herein report the identification of the UA20 antigen as human CD46, a negative regulator of the innate immune system (the complement cascade). We further performed genomic and proteomic studies to establish that CD46 is a functional antigen that is highly expressed in mCRPC, including both adenocarcinoma and neuroendocrine subtypes that have acquired abiraterone and/or enzalutamide resistance. We studied the internalizing pathway of our anti-CD46 antibodies and identified a mechanism of tumor-selective entry via macropinocytosis. We further developed a novel macropinocytosing CD46 antibody-drug conjugate (ADC) and showed potent antitumor activity in vitro and in vivo. To enable translation to the clinic, we determined that our anti-CD46 antibody has excellent tissue specificity, binding mainly to placental trophoblasts and prostate epithelium but not other normal tissues. Exploratory toxicology (tox) study in nonhuman primates showed no on-target toxicity, supporting translational development of our novel CD46 ADC for mCRPC treatment.

Results

CD46 identified as the target antigen bound by our anti-prostate cancer human antibody. We have previously developed a method to identify novel human antibodies targeting cancer cell surface antigens expressed by tumor cells in situ residing in their tissue microenvironment by selecting phage antibody display libraries directly on cancer patient specimens with the aid of LCM (24, 25). Among the panel of antibodies identified, UA20 displayed excellent tumor-targeting property in vivo (26) and possessed the 3 properties that the original selection was designed to capture: binding to tumor specimens, internalizing, and recognizing native epitopes and thus living tumor cells (24). In order to identify the cell surface antigen bound by UA20, we performed IP and mass spectrometry analysis on cell lysates prepared from surface biotin-labeled prostate cancer cell line DU145. Silver-stained SDS-PAGE gel showed 2 prominent bands between 55 and 72 kDa (Supplemental Figure 1A; supplemental material available online with this article; https://doi.org/10.1172/jci.insight.121497DS1) that also corresponded to 2 bands on the Western blot that identified them as membrane proteins (Supplemental Figure 1B). Both bands were identified by mass spectrometry analysis as human CD46, or membrane cofactor protein (MCP), consistent with what is known about the gel migration pattern of this highly glycosylated membrane protein (27). We next performed 2 experiments to independently verify this target identification. (i) We repeated the pull-down experiment using cell lysates from DU145 that is bound by UA20 and BPH-1 (control, not bound by UA20) and analyzed the IP product by Western blotting using a commercially available mouse mAb against human CD46 (Figure 1A). (ii) We ectopically expressed human CD46 in CHO-K1 cells and analyzed UA20 binding by FACS. As shown in Figure 1B, UA20 binds specifically to human CD46-transfected but not nontransfected CHO cells. Taken together, these data confirm that human CD46 is the cell surface antigen bound by UA20.

We next sought to determine the epitope bound by UA20. The extracellular portion of human CD46 consists of 4 domains known as complement control protein repeats (CCPs) or Sushi domains, followed by a serine/threonine/proline-rich (STP) region (Supplemental Figure 1C). The best known function of CD46 is negative regulation of the innate immunity, i.e., inhibition of the complement cascade. CCP3 and CCP4 are the main complement-binding sites, along with a small region on CCP2. CD46 is also a receptor for a laboratory strain oncolytic measles virus that binds to CCP1 and CCP2. To identify the CD46 epitope bound by UA20, we created deletion mutants with CCP1 and -2 deleted (De1+2), CCP1 deleted (De1), CCP2 deleted (De2), CCP3 deleted (De3), and CCP4 deleted (De4). As shown in Figure 1C, deletion of CCP3 or CCP4 did not have a significant effect on UA20 binding to CD46. In contrast, deletion of both CCP1 and CCP2 resulted in a total loss of binding. Deletion of CCP1 or 2 alone resulted in partial loss of binding (Figure 1C). In addition, we determined that UA20 binds to a conformational epitope, as it does not bind to the denatured CD46 protein on Western blot. These data suggest that UA20 binds to a conformational epitope formed within CCP1 and CCP2.

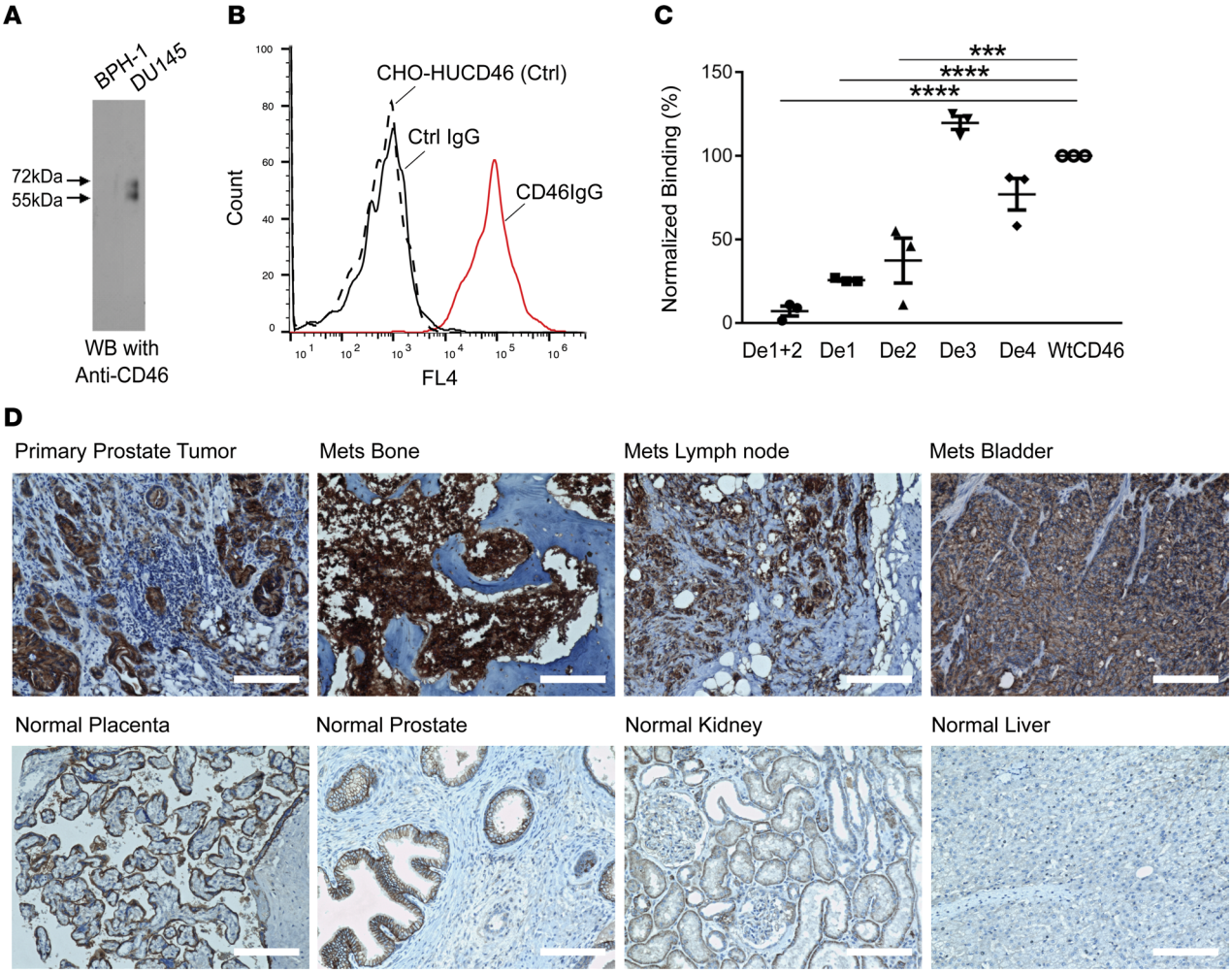

Figure 1. Identification of human CD46 as a target for prostate cancer. (**A**) Verification of CD46 as the target antigen by IP and Western blot analysis using validated anti–human CD46 antibody. Two bands characteristic of human CD46 were seen in IP products from tumor (DU145) but not control nontumorigenic cells (BPH-1). CD46 is known to migrate on SDS-PAGE as 2 bands (27). (**B**) Verification of target identification by antibody binding to cells ectopically expressing human CD46. CHO-HUCD46: control (Ctrl), CHO-K1 cells transiently transfected with human CD46 expression plasmid without antibody incubation. Ctrl IgG: a nonbinding antibody randomly picked from naive library was incubated with CHO-HUCD46. CD46IgG: UA20 IgG was incubated with CHO-HUCD46 cell-sn. (**C**) Epitope mapping by ectopic expression of CD46 deletion constructions followed by FACS analysis. De1+2, CD46 with Sushi domains 1 and 2 deleted. De1, domain 1 deleted. De2, domain 2 deleted. De3, domain 3 deleted. De4, domain 4 deleted. WtCD46: full-length WT CD46 that was used for normalization of FACS binding data. ***$P < 0.001$ ($P = 0.0002$), ****$P < 0.0001$. One-way ANOVA, Bonferroni's multiple comparisons test. The experiment was done in triplicate. (**D**) IHC study of formalin fixed, paraffin-embedded prostate cancer tissues and a normal human tissue array. Top row: primary tumor and mCRPC samples with strong positive staining signals. H score for primary tumor, 211; bone mets (Mets), 295; lymph node mets 202; and bladder mets 276. Bottom row: normal tissues staining. Placental trophoblasts showed positive signals, along with prostate epithelium. Weak staining was seen for kidney and liver. H score for placenta, 167; prostate epithelium, 142; kidney, 52; and liver 12. Scale bars: 150 μm.

We next determined that the UA20 epitope is an internalizing CD46 epitope. We performed a functional internalization assay by assessing UA20-mediated internalization and cytotoxicity of a plant toxin, saporin, that lacks a cell entry mechanism on its own (28, 29). We formed the UA20 immunotoxin by mixing biotinylated UA20 with streptavidin-saporin (ZAP) at a 1:1 molar ratio. We used the mCRPC line LNCaP-C4-2B, which expresses CD46, for the cytotoxicity assay, along with 2 nontumorigenic control cell lines, BPH-1 (benign prostatic hyperplasia epithelial cell line) and HS775Li (a primary normal human liver cell line), that express low or nondetectable amount of human CD46 (Supplemental Figure 2A). As shown in Supplemental Figure 2B, the UA20 immunotoxin potently (EC_{50} 170 ± 36 pM) and specifically killed LNCaP C4-2B, but not BPH-1 and HS775Li, cells. These data suggest that CD46 can be targeted for intracellular payload delivery and for development of novel therapeutics such as ADCs.

Evaluation of CD46 expression in tumor and normal human tissue. The first step in validating CD46 as a therapeutic target was to study tissue specificity of CD46 expression. We have previously reported,

before identification of the target antigen, results of an IHC study on frozen primary prostate cancer tissues, where we found positive staining in all cases (24). To broaden applicability, we performed additional IHC studies on formalin-fixed, paraffin-embedded (FFPE) prostate cancer tissues using the H-294 rabbit antibody, which has been used as a biomarker for oncolytic measles virus trials (30). Two sets of tissues were studied. One was a primary prostate cancer tissue array from 36 cases, and the other mCRPC specimens from 15 cases. 100% (36 of 36) of primary prostate tumors expressed CD46, with 80.56% (29 of 36) showing strong staining (an example shown in Figure 1D, top row, far left). Low or no staining was found in adjacent normal tissues and in infiltrating lymphocytes (Figure 1D; additional close-up views shown in Supplemental Figure 3). On mCRPC tissues containing metastasis to the bone, lymph node, bladder, and liver, positive staining was found in all samples, with 13 of 15 being strongly positive (examples shown in Figure 1D, top row, three right; additional close-up views shown in Supplemental Figure 3). Thus, CD46 protein is highly expressed in both primary and metastatic castration-resistant prostate cancer.

We next studied CD46 protein expression in normal human tissues by IHC. An FFPE human normal tissue array containing 66 cases of 33 normal organ/tissue was stained with the anti-CD46 rabbit antibody H-294. Notable expression was observed in placental trophoblasts and to a lesser degree prostate epithelium (Figure 1D, bottom row; additional close-up views shown in Supplemental Figure 4). Weak staining was observed in the stomach, liver, kidney, small intestine, and rectum (examples shown in Figure 1D, bottom row). Other normal tissues showed no notable CD46 staining. Thus, CD46 protein expression appears to have good tissue specificity.

Taken together, the results of our IHC study on both tumor and normal FFPE tissues show that CD46 is nearly uniformly overexpressed in both primary and metastasis prostate cancers, with weak or no expression observed in most normal tissues, except for placental trophoblasts and to a lesser degree normal prostate epithelium.

Identification and evaluation of a panel of CD46-specific human mAbs for therapeutic development. To identify and optimize a lead antibody for therapeutic targeting of CD46, we performed both phage and yeast antibody display library selection using methods that we described previously (31, 32). More than 20 unique human scFvs were identified that bind to Sushi domains 1 and 2 of CD46. Following conversion of scFv into full-length human IgG1 and characterization of binding specificity, affinity, internalization, and production level in mammalian expression system, 5 IgG1s were selected for further study. Competition experiment showed that these antibodies fall into 2 major epitope groups, with YS5, YS12, and 3G8 in one (overlapping with the UA20 epitope), and HGNY in another (Supplemental Figure 5A). None of the antibodies interfered with binding of complement element C3b to CD46 (Supplemental Figure 5B), which was expected, as C3b binds to Sushi domains 3 and 4. YS5, YS12, and to a lesser degree HGNY IgG1s showed a partial epitope overlap with the oncolytic measles virus H protein (Supplemental Figure 5C), which mediates viral entry into target cells by macropinocytosis.

The YS5 IgG1 showed about 1 nM apparent K_D on prostate cancer cells (Figure 2A, left). On normal human primary prostate epithelial cells, YS5 IgG1 had an apparent K_D of 9.67 ± 0.74 nM (Figure 2A, middle). It showed a similar apparent K_D (6.75 ± 1.98 nM) on primary cynomolgus monkey prostate epithelial cells (Figure 2A, right), thus identifying the cynomolgus monkey as an appropriate nonhuman primate species for toxicology studies.

We selected YS5 as our lead human antibody for translation development due to its high-affinity binding to tumor cells, cross-species binding, internalization, favorable hydrophobicity profile on HPLC, high production yield in HEK293 cells, and excellent thermal stability. Like UA20, YS5 binds to a conformational epitope formed within Sushi domains 1 and 2. It does not bind to denatured protein but recognizes CD46 in its native conformation on living cell surface. We biotin-labeled YS5 IgG1 and performed a comprehensive IHC study on an FDA standard frozen human tissue panel for therapeutic antibody evaluation. This array contains 89 cases from 28 normal organs/tissues (see Figure 2B for the organ/tissue list). A summary of staining results is shown in Figure 2B, with representative images in Figure 2C (additional close-up views shown in Supplemental Figures 6–8). Other than placental trophoblasts and to a lesser degree prostate epithelium, YS5 showed either weak or no staining in normal human tissues. These data are consistent with the IHC data we obtained from FFPE tissues shown in Figure 1D. Most important, they show that our lead antibody, YS5, has a high degree of tissue specificity, making it likely that a therapeutic built on YS5 will have an excellent therapeutic window.

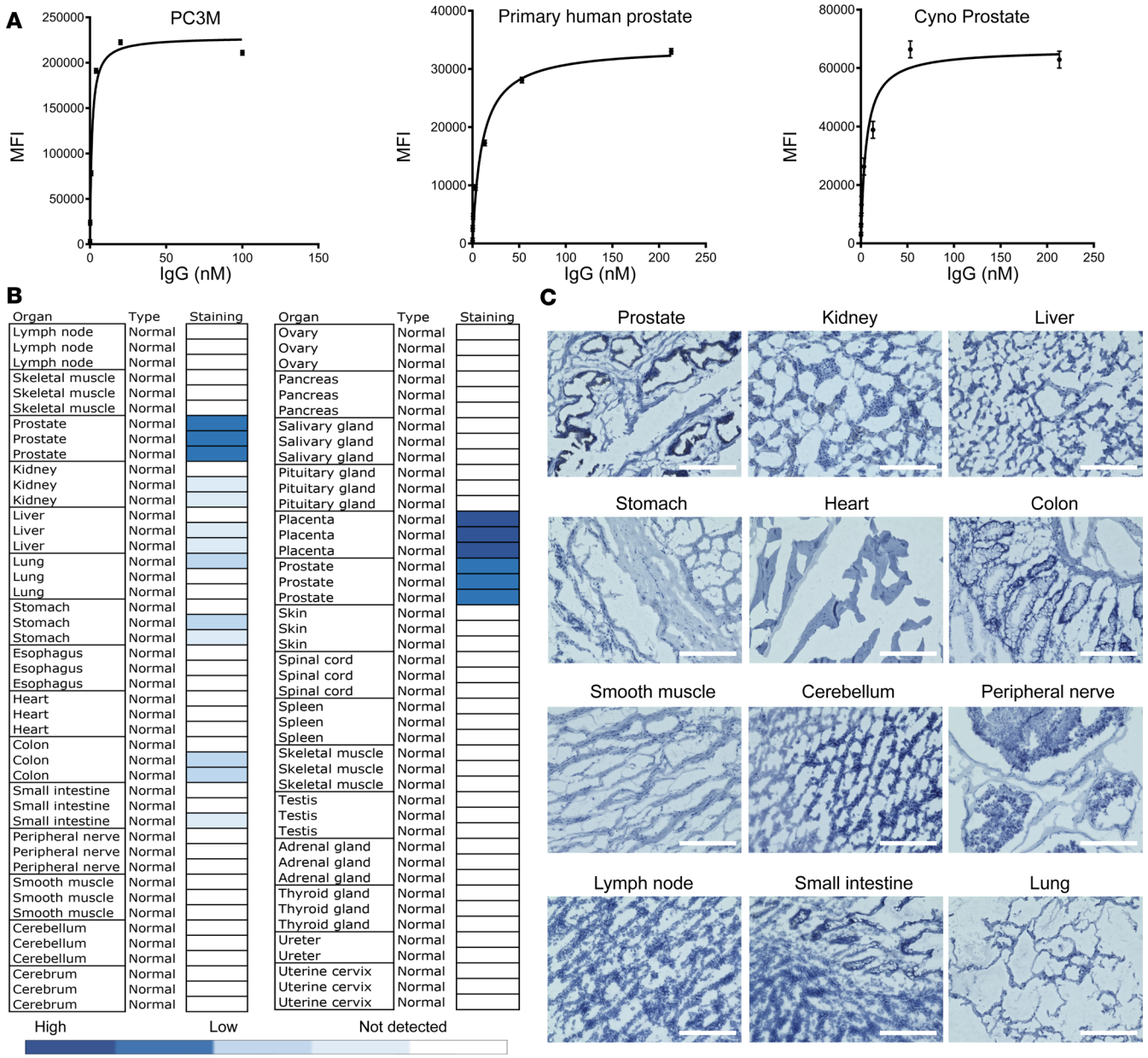

Figure 2. Antibody binding to tumor and normal cells and tissues. (**A**) Apparent K_D measurement by FACS of YS5 IgG1 on prostate cancer (PC3M, apparent K_D = 1.186 ± 0.295 nM), human primary normal prostate epithelial cells (HPrEpC, apparent K_D = 9.666 ± 0.738 nM), and primary cynomolgus monkey prostate epithelial cells (Cyno Prostate, apparent K_D = 6.748 ± 1.979 nM). (**B**) IHC staining patterns of YS5 IgG1 on FDA standard human normal tissue panel for therapeutic antibody evaluation. (**C**) Images of normal tissue staining described in **B**. H score for prostate epithelium, 173; kidney, 4; liver, 2; colon, 1.5; small intestine, 1.6; stomach, 1.6; and the rest, 0. Scale bars: 200 μm.

Tumor-selective internalization via macropinocytosis. We have previously used ND70 as a macropinocytic marker to study pathways of antibody internalization (21, 23). Oncolytic measles virus is known to enter cells via macropinocytosis (33). As a positive control, we showed that the oncolytic measles virus H protein was internalized by DU145 cells, colocalized with ND70, confirming its pathway of internalization via macropinocytosis (Supplemental Figure 9). As our anti-CD46 antibody YS5 and H protein bind to an overlapping epitope on CD46, we hypothesized that our YS5 IgG1 may enter cell via macropinocytosis, an inherently tumor-selective pathway for cellular entry (34–36). We thus studied YS5 internalization by tumor and normal cells. YS5 IgG1 was incubated with mCRPC lines (LNCaP-C4-2B, DU145, and PC3M) and control $CD3^+$ human primary T cells for 4 and 24 hours. Colocalization with ND70 was studied by confocal microscopy. As shown in Figure 3A (4 hours) and Supplemental Figure 10 (24 hours), in all 3 mCRPC

lines studied, the anti-CD46 mAb YS5 was internalized in a time dependent manner and colocalized with ND70. To further evaluate antibody localization to specific subcellular compartments, we studied YS5 co-localization with lysosomes marked by lysosomal-associated membrane proteins (LAMP-1). Colocalization of YS5 and LAMP-1 was observed in all mCRPC lines following 4 h incubation (Supplemental Figure 11), suggesting an efficient routing of the antibody to the lysosomal compartment, a preferred place for intracellular delivery of ADC where the antibody component can be processed to release the drug (37). For normal cells such as primary T cells, no notable ND70 uptake was observed at either 4 (Figure 3A) or 24 hours (Supplemental Figure 12A), suggesting a lack of macropinocytosis activity. No YS5 uptake was observed by normal T cells at either 4 or 24 hours (Figure 3A and Supplemental Figure 12B), suggesting a tumor-selective mode of internalization for our anti-CD46 antibody.

CD46 ADC development and selective tumor cell cytotoxicity in vitro. We next conjugated the auristatin derivative monomethyl auristatin phenylalanine (MMAF) to YS5 IgG1 using the maleimidocaproyl valine-citrulline linker (MC-vc-PAB) to create the CD46 ADC. HPLC analysis showed that on average 3.3 MMAF molecules were conjugated to YS5 IgG1 (Supplemental Figure 13A). Conjugation with MMAF did not alter the antibody binding property (Supplemental Figure 13B). A control ADC was also created using a nonbinding human IgG1 with a similar drug-to-antibody ratio (Supplemental Figure 13A). CD46 and control ADCs were tested for cytotoxicity in vitro against a panel of human mCRPC lines (LNCaP-C4-2B, DU145, and PC3M) and control cells (BPH-1, $CD3^+$ human T cells, and CD14-depleted human PMBCs). As shown in Figure 3B, our CD46 ADC showed potent cytotoxicity against all mCRPC lines studied with EC_{50} values between 275 pM and 1.13 nM (EC_{50} 275 ± 98 pM for LNCaP-C4-2B, 1.13 ± 0.45 nM for DU145, and 607 ± 172 pM for PC3M). In contrast, CD46 ADC showed no on-target cytotoxicity against control cells (Figure 3B, bottom panels). Control ADC also showed little effect on any cells studied (Figure 3B), suggesting that the observed cytotoxicity for tumor cells was due to CD46 targeting and internalization by CD46 ADC.

Evaluation of in vivo antitumor efficacy of CD46 ADC. We evaluated CD46 ADC in both subcutaneous (subcu) and intrafemoral xenograft models bearing the mCRPC line LNCaP-C4-2B. In the subcu xenograft model, animals were randomized into study groups on day 21 after graft with a mean tumor size greater than 500 mm^3 in each group (n = 5), and treated i.v. with 4 doses of 5 mg/kg CD46 ADC, control naked mAb, control ADC, and the vehicle (PBS). As shown in Figure 4A, the CD46 ADC produced a robust antitumor effect, resulting in complete remission and no palpable tumor at the site of implantation until the end of the experiment (45 days after the first dosing or day 66 after the initial graft). In contrast, no notable antitumor effects were observed for any of the control groups (Figure 4A). Body weight was monitored during the course of the study, and no notable loss (>15%) was observed (Figure 4B).

Next, we engineered an LNCaP-C4-2B line that expresses the firefly luciferase gene (LNCaP-C4-2B-Luc) and grafted it intrafemorally into NSG mice to evaluate anti-tumor activity of the CD46 ADC. Mice were treated on day 7 with the CD46 ADC or control ADC at 4 mg/kg every 4 days for a total of 4 injections (q4d × 4) (Figure 4C). CD46 ADC eliminated bioluminescence signals by day 30, and the effect lasted until the end of the experiment (day 65) (Figure 4D). In contrast, control ADC showed no antitumor effect, as evidenced by a continued increase in bioluminescence signal (Figure 4E). There was no significant change in body weights of treated animals during the course of the experiment (Supplemental Figure 14).

Genomic and clinical data supporting CD46 as a novel target for mCRPC. To evaluate the genomic status of the CD46 gene in prostate cancer, we studied the public database cBioPortal (http://www.cbioportal.org/) (38, 39) for both primary and mCRPC patient samples (7, 38, 40–45). As shown in Figure 5A, independent datasets from multiple centers (1,050 patient samples) showed about 7% CD46 genomic gain in primary tumor and 38% in mCRPC patients prior to abiraterone and enzalutamide treatment. In one dataset (WCM 2016, Figure 5A) enriched for NEPC (7), CD46 genomic gain was seen in 50.5% of cases. We also analyzed CD46 gene genomic copy number in mCRPC patient biopsies collected by the Prostate Cancer West Coast Dream Team (46) and found CD46 genomic copy number gain in 30.77% of abiraterone-naive patients (4 of 13) and 45.45% in abiraterone-resistant patients (5 of 11). These data suggest that there is a progressive gain in CD46 genomic copy number as the disease progresses from primary to metastasis, and from abiraterone naive to abiraterone resistant.

In addition to genomic copy number gain, RNA sequencing (RNA-Seq) data from patient samples (cBioPortal) showed that the CD46 mRNA expression level was significantly higher in samples with copy number gain/amplification (Figure 5B). In addition to the public database, we studied CD46 mRNA expression from an RNA-Seq database developed by the West Coast Dream Team. CD46

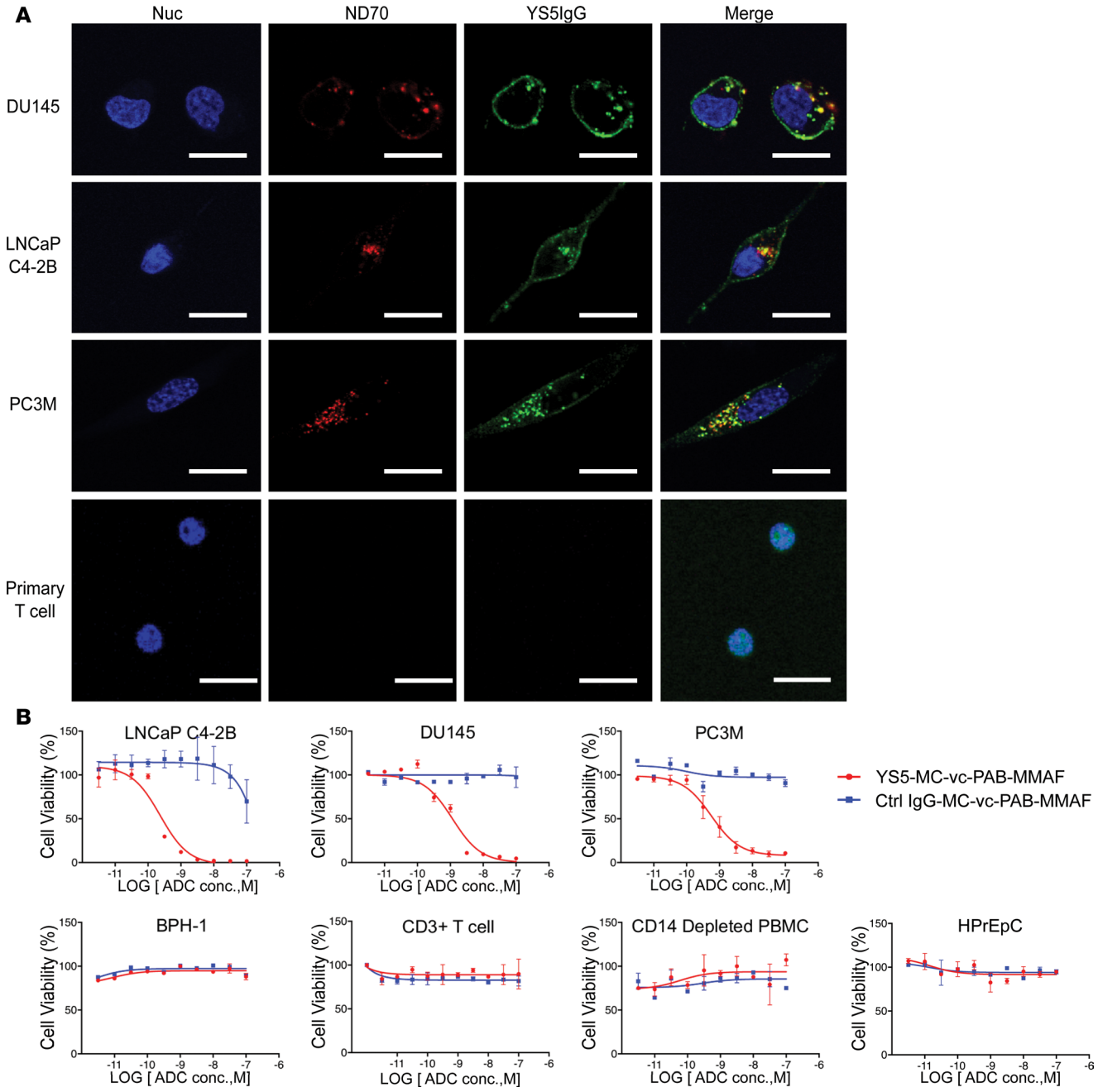

Figure 3. Internalization by macropinocytosis and tumor-selective killing by CD46 ADC. (**A**) Confocal microscopy study of YS5 IgG1 internalization into mCRPC lines (DU145, LNCaP-C4-2B, and PC3M) and primary human T cells. Colocalization between the macropinocytosis marker ND70 and YS5 IgG1 is analyzed in a single confocal slice. The rate of colocalization, calculated as the percentage of double-positive intracellular spots relative to antibody-positive intracellular spots, was 93.75% (15 of 16) for DU145, 94.44% (LNCaP-C4-2B), and 92.68% (38 of 41) for PC3M. There was no internalization and no colocalization for primary T cells. In the above experiment, the BPH-1 cell line was used as a negative control (no YS5 binding and no fluorescence signal; data not shown). Nuc, nuclei. Scale bars: 30 μm. (**B**) In vitro tumor killing assay by CD46 ADC. YS5-MC-vc-PAB-MMAF was incubated with a panel of mCRPC lines (LNCaP-C4-2B, DU145, and PC3M) and control normal human cells (BPH-1, $CD3^+$ T cells, and CD14-depleted PBMCs, and the normal human primary prostate epithelial cell line HPrEpC). A nonbinding human IgG1 was conjugated to MMAF and used as a control. EC_{50} values were 275 ± 98 pM for LNCaP-C4-2B; 1.13 ± 0.45 nM for DU145; and 607 ± 172 pM for PC3M. No cytotoxic effects were observed on the panel of control normal cells studied across the ADC concentration (conc.) range.

mRNA was overexpressed in mCRPC adenocarcinoma at levels significantly higher than prostate-specific membrane antigen (PSMA) (Figure 5C), a current target for clinical antibody therapy development in mCRPC. Unlike PSMA, CD46 showed a rather uniform mRNA expression level in mCRPC samples (Figure 5C). Furthermore, CD46 was highly expressed across prostate cancer subtypes, including the

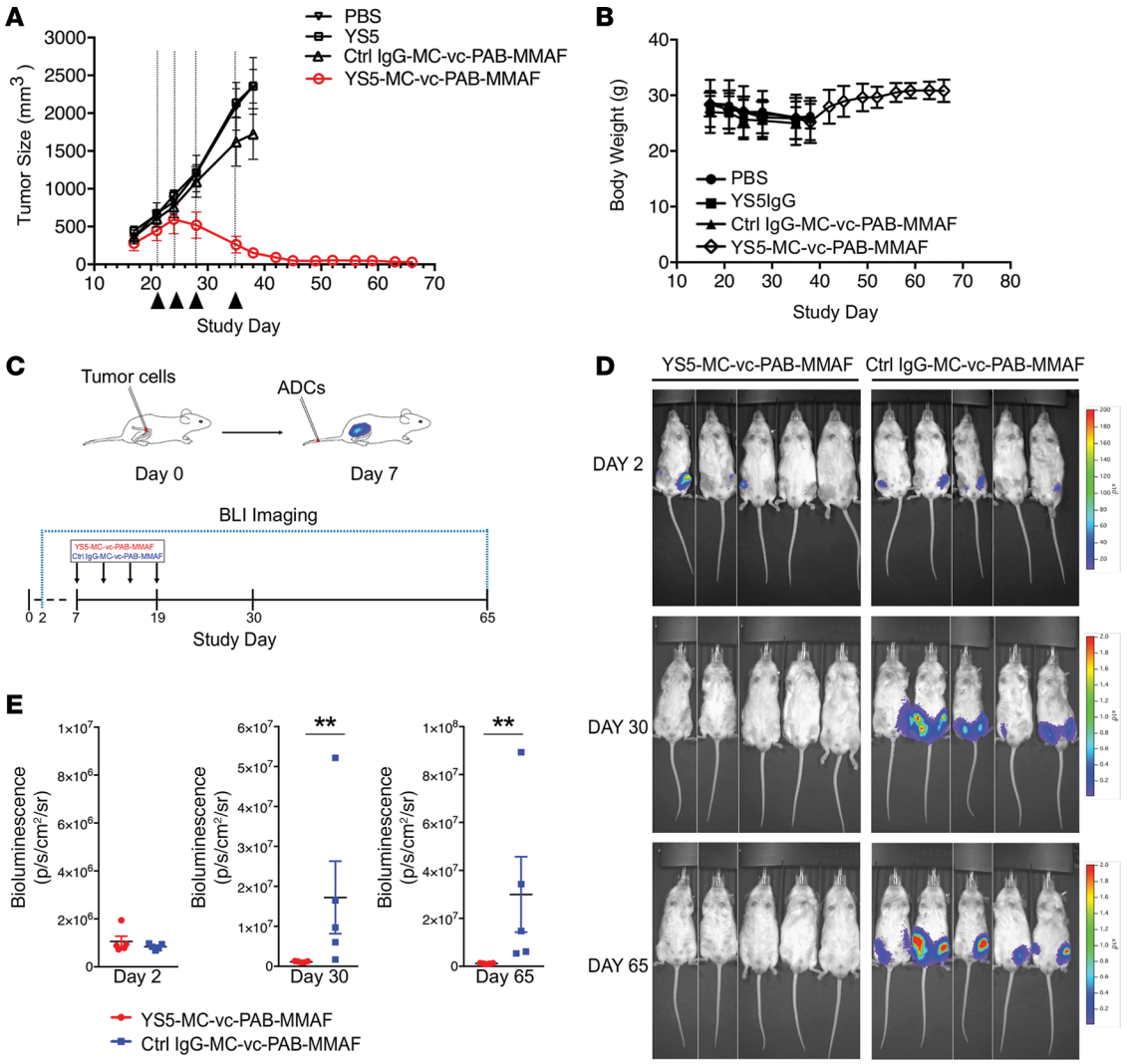

Figure 4. CD46 ADC potently inhibits mCRPC xenograft growth in vivo. (**A**) Large-sized (~500 mm^3) LNCaP-C4-2B xenograft was treated with YS5-MC-vc-PAB-MMAF for a total of 4 doses at 5 mg/kg. Three control arms were included: vehicle only (PBS), naked antibody (YS5), and control ADC based on a nonbinding IgG1 (Ctrl IgG-MC-vc-PAB-MMAF). Injection days are indicated by black triangles and dashed lines. (**B**) Body weight assessment during the course of the experiment shown in **A**. (**C**) Study design of ADC treatment of intrafemorally grafted mCRPC. LNCaP-C4-2B engineered to express the firefly luciferase gene was injected intrafemorally. Graft was allowed to establish and grow for 7 days, and CD46 ADC was injected at 5 mg/kg for a total of 4 doses. (**D**) Bioluminescence imaging (BLI) showed that CD46 ADC potently eliminates intrafemorally grafted mCRPC cell line xenograft model. (**E**) Quantification of BLI (CD46 ADC, i.e., YS5-MC-vc-PAB-MMAF, vs. control ADC, i.e., Ctrl IgG-MC-vc-PAB-MMAF) on day 2 (no significant difference), day 30 (**$P < 0.01$, $P = 0.0079$), and day 65 (**$P < 0.01$, $P = 0.0079$). Mann-Whitney U nonparametric test, unpaired, 2-tailed.

treatment-induced neuroendocrine/small cell subtype (Figure 5D). In abiraterone-resistant patients, CD46 maintained the high expression level (Figure 5E). In the abiraterone/enzalutamide-resistant neuroendocrine/small cell subtype, the CD46 mRNA level was significantly higher than that of PSMA (Figure 5F). This result, which is based on analysis of the West Coast Dream Team data, is consistent with our finding (Supplemental Table 1) from mining a previously published database (7); i.e., PSMA expression was drastically reduced in NEPC, but CD46 expression was maintained at a high level across tumor subtypes.

To assess CD46 protein levels in mCRPC patient samples, we studied cell surface CD46 expression in circulating tumor cells (CTCs) from both abiraterone/enzalutamide-naive and -resistant patients (patient information is shown in Supplemental Table 2). We found that CD46 was expressed by CTCs and at much higher levels than non-CTC white blood cells (Figure 5G). Interestingly, CTCs from abiraterone- or enzalutamide-resistant patients showed a much higher level of cell surface CD46 expression compared with CTCs from naive patients (Figure 5G).

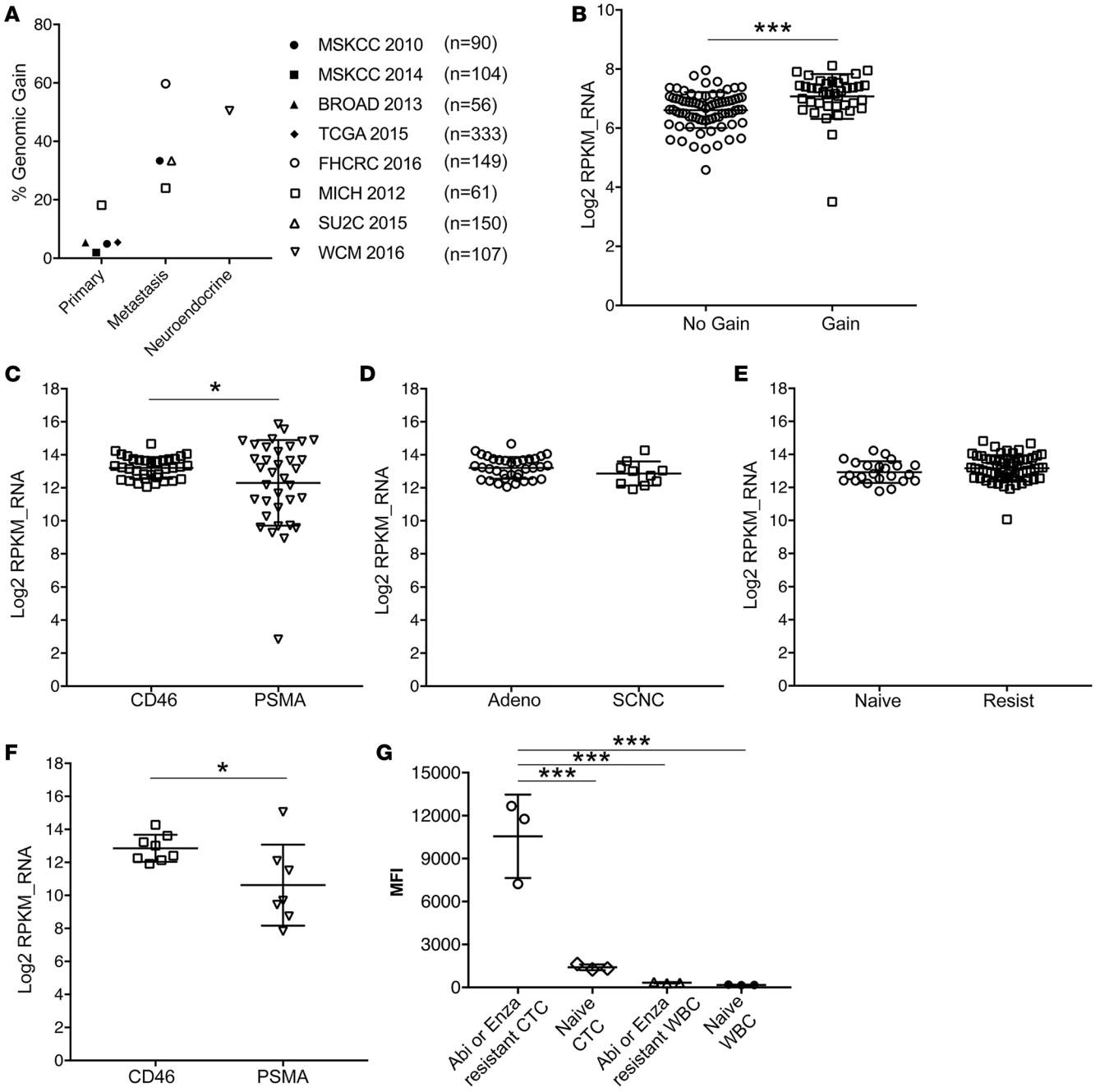

Figure 5. CD46 gene expression and genomic change in mCRPC. (**A**) Compared with primary tumor, mCRPC patient samples show increased CD46 genomic gain/amplification (7.16% ± 2.83% for primary vs. 37.60% ± 7.70% for metastasis). Data are from a public database (http://www.cbioportal.org). Studies were conducted by multiple centers, as indicated. The number of patient samples in each dataset is indicated. MSKCC, Memorial Sloan Kettering Cancer Center; BROAD, Broad Institute; TCGA, The Cancer Genome Atlas; FHCRC, Fred Hutchinson Cancer Research Center; MICH, University of Michigan; SU2C, Stand Up To Cancer; WCM, Weill Cornell Medicine. (**B**) Prostate cancer patients who have undergone CD46 genomic gain/amplification show significantly higher levels of CD46 mRNA expression. ***$P < 0.001$ ($P = 0.0005$). Student's t test, unpaired 2-tailed. (**C**) In mCRPC adenocarcinoma, CD46 is homogeneously overexpressed, and at a level significantly higher than that of PSMA. *$P < 0.05$ ($P = 0.040$). Student's t test, paired, 2-tailed. The analysis was performed on the dataset generated by one center (41). Due to differences in data format, we could not perform a combined analysis using datasets from all centers. (**D**) CD46 mRNA is overexpressed across prostate cancer subtypes (adenocarcinoma [Adeno] and neuroendocrine-like subtypes; no significant difference). SCNC, small cell/neuroendocrine carcinoma. (**E**) Abiraterone-resistant patients maintained high CD46 mRNA expression (no significant difference between ASI-naive and -resistant). (**F**) In neuroendocrine mCRPC that is resistant to ASIs, CD46 mRNA level is significantly higher than PSMA. *$P < 0.05$ ($P = 0.030$). Student's t test, paired, 2-tailed. (**G**) Cell surface CD46 level is upregulated in CTCs compared with WBC and is further upregulated in CTCs from ASI-resistant compared with -naive patients. Abi, abiraterone; Enza, enzalutamide; MFI, median fluorescence intensity. ***$P <$ 0.001. One-way ANOVA, Bonferroni's multiple comparisons test.

CD46 expression in NEPC. The aforementioned RNA-Seq data support CD46 as a target for NEPC, including small cells that are differentiated from adenocarcinoma as they acquire resistance to AR pathway inhibition. We sought to evaluate CD46 expression in mCRPC lines that were induced to differentiate from the adenocarcinoma to neuroendocrine-like subtype. LNCaP-C4-2B cells were cultured for 5 days in conditioned medium (CM) of the bone marrow stromal HS5 cell line (47), and CD46 expression was measured by quantitative FACS, with cell surface antigen copy number determined. CD46 antigen density doubled when cultured in HS5 CM (Supplemental Figure 15A). The cocultured LNCaP-C4-2B cells underwent a change in morphology by developing long and narrow branches, and increasing the expression of neuron-specific enolase (NSE, a neuroendocrine marker) by Western blot analysis (Supplemental Figure 15B), suggesting that these cells underwent neuroendocrine differentiation.

To further connect CD46 to NEPC, we performed an IHC study and found strong CD46 staining on NSE-positive prostate cancer cells (Supplemental Figure 15C; additional close-up views shown in Supplemental Figure 16). To move from descriptive to functional studies with regard to the targetability of CD46 in NEPC, we studied an AR-negative NEPC cell line, H660, that was derived from a metastatic site of an extrapulmonary small cell carcinoma arising from the prostate (48). Unlike PSMA, CD46 was expressed at high levels on H660 cell surface (Figure 6A), with antigen density greater than 520,000 per cell (Figure 6B, CD46, 520,430 ± 52,020 vs. PSMA, 23,733 ± 8,591). Western blot analysis confirmed high CD46 expression and NSE expression by H660 (Figure 6C). To determine whether our anti-CD46 antibody YS5 is internalized by H660 cells, we performed a confocal microscopy study to assess YS5 internalization and intracellular trafficking after internalization. We found that YS5 was internalized by H660 cells by macropinocytosis (Figure 6D for 4-hour and Supplemental Figure 17 for 24-hour incubation, colocalization with ND70) and was routed to lysosomes following 4- and 24-hour incubation (Supplemental Figure 18). We next studied the cytotoxicity of CD46 ADC for H660 cells in vitro and found a potent cytotoxic effect (Figure 6E). Collectively, our data show that NEPC cells express high levels of CD46, which has the potential to be an excellent target for therapy development against this subtype of mCRPC.

Enhanced anti-mCRPC effect by CD46 ADC following AR inhibitor treatment. The above clinical data analysis provide correlative evidence of upregulation of CD46 gene expression upon application of abiraterone and other ASIs. To evaluate whether CD46 expression correlates with abiraterone/enzalutamide resistance in a cell-based in vitro model, we treated LNCaP-C4-2B cells with either abiraterone or enzalutamide and determined the cell surface CD46 level (antigen density) by quantitative FACS. Both abiraterone and enzalutamide treatments more than doubled the level of CD46 cell surface expression (Figure 6, F and G, respectively), increasing from 163,548 ± 6,402 before treatment to 336,690 ± 11,064 (abiraterone-treated) or 365,058 ± 42,168 (enzalutamide-treated). This ASI treatment–induced CD46 upregulation was also observed for 2 additional mCRPC cell lines, DU145 and VCaP (Supplemental Figure 19), suggesting that this is a rather general phenomenon. We next studied whether the increase in CD46 surface expression results in enhanced sensitivity of mCRPC cells to CD46 ADC. In this experiment, we first exposed LNCaP-C4-2B cells to 10 μM abiraterone to induce CD46 upregulation, removed the drug, and then exposed the cells to CD46 ADC. As shown in Figure 6H, abiraterone-induced upregulation of CD46 rendered mCRPC cells more sensitive to CD46 ADC, with EC_{50} decreasing by 17-fold (EC_{50} 226 ± 103 pM vs. 13 ± 1.8 pM).

Exploratory tox study of CD46 ADC in nonhuman primate. As a preliminary assessment of translation potential of our CD46 ADC, we performed an exploratory tox study in the cynomolgus monkey, as we found that YS5 IgG1 binds with similar affinity to human and cynomolgus CD46 (see Figure 2A). We tested 3 doses in both male (n = 2 for each dose, total 6) and female (n = 2 for each dose, total 6) animals: 0 mg/kg (control), 1 mg/kg, and 5 mg/kg, via a single bolus i.v. injection. Body weight was monitored on day –3 (3 days before the first injection), –1, 7, and 14. As shown in Figure 7A, no significant body weight loss (>15%) was found in any dose range tested. Blood samples were collected on days –3, 2, 9, and 15. Absolute neutrophil counts were determined, and no major change was observed (Figure 7B, and Supplemental Figure 20A [male] and Supplemental Figure 20B [female]). A mild transient increase in liver enzyme activities (aspartate transaminase [AST] and alanine transaminase [ALT]) was found, peaking on day 7 and returning to baseline on day 15 (Figure 7, C and D), consistent with the drug-related toxicity observed for other MMAF-based ADCs (49). No difference between males and females was observed for either AST (Supplemental Figure 21, A and B) or ALT (Supplemental Figure 21, C and D). The experiment was terminated on day 15, and major organs were harvested for necropsy analysis. No obvious on-target toxicity was observed for any doses tested (Figure 7E). At the highest dose tested, a mild increase

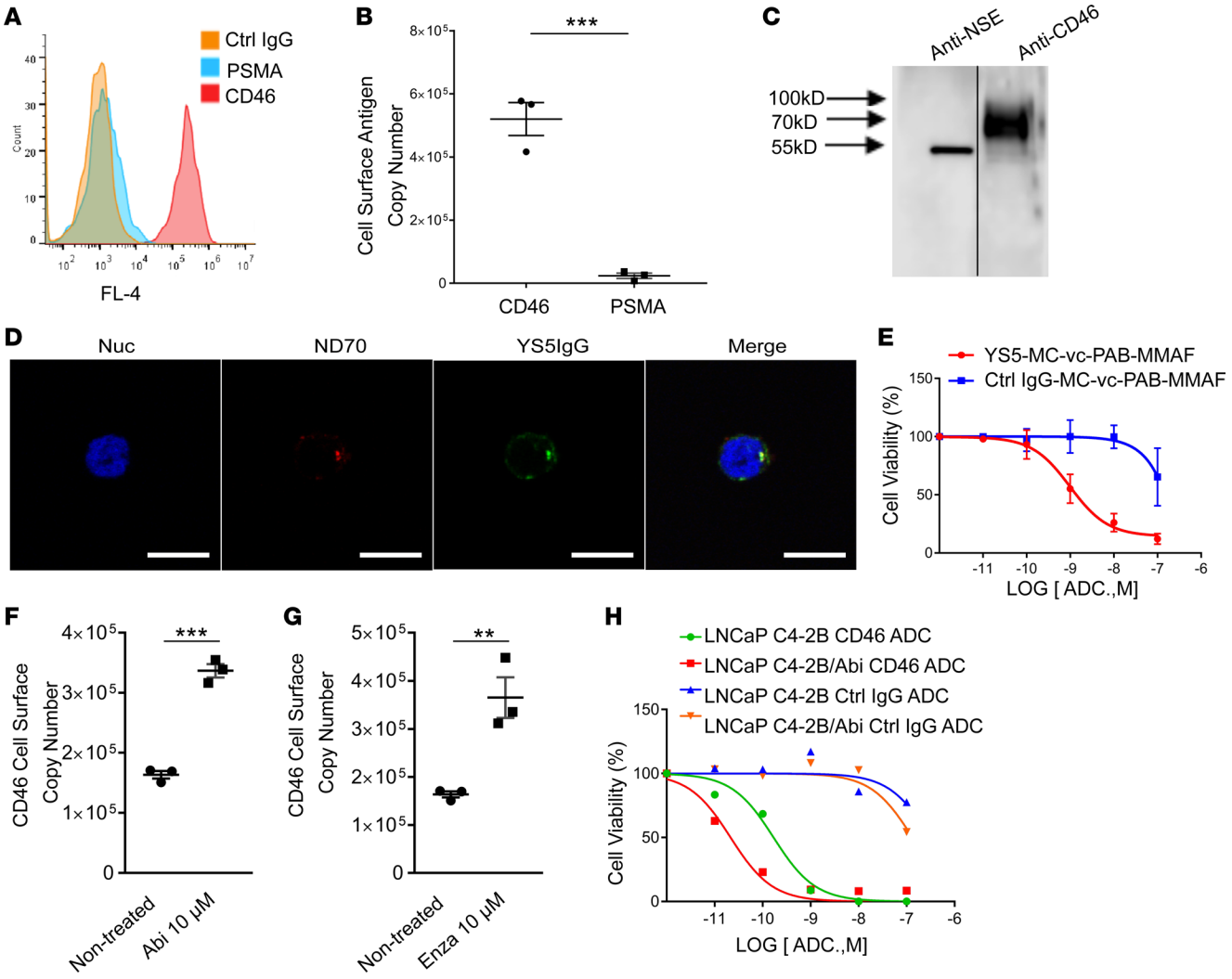

Figure 6. Neuroendocrine and ASI-resistant prostate cancer cells upregulate cell surface CD46 expression, and exhibit enhanced sensitivity to CD46 ADC. (**A–E**) CD46 is highly expressed on the surface of the NEPC cell line H660, and H660 is sensitive to CD46 ADC. (**F–H**) Upregulation of CD46 and enhanced sensitivity to CD46 ADC by ASI-resistant mCRPC cells. (**A**) FACS analysis of CD46 and PSMA expression on H660. (**B**) Antigen density (surface copy number per cell) for CD46 and PSMA on H660 cell (520,430 ± 52,020 for CD46 vs. 23,733 ± 8,591 for PSMA). ***$P < 0.01$ ($P = 0.0007$), Student's t test, unpaired, 2-tailed; triplicate. (**C**) Western blot analysis showed CD46 protein expression as well as the neuroendocrine marker neuron-specific enolase (NSE). (**D**) YS5 IgG1 is internalized by H660 cells via macropinocytosis (colocalization with ND70) during 4-hour incubation at 37°C. The rate of colocalization was 83.33% (5/6). Scale bars: 30 μm. (**E**) CD46 ADC potently kills the neuroendocrine cancer line H660 in vitro (EC_{50} 796 ± 460 pM). (**F–H**) CD46 antigen density increases in LNCaP-C4-2B cells following incubation with abiraterone (**F**) and enzalutamide (**G**) for 7 days, rising from 163,548 ± 6,402 before treatment to 336,690 ± 11,064 and 365,058 ± 42,168, respectively. ***$P < 0.05$ ($P = 0.0002$) (**F**) and **$P < 0.01$ ($P = 0.0091$) (**G**); Student's t test, unpaired, 2-tailed; triplicate. The increased CD46 antigen density leads to increased sensitivity to CD46 ADC (**H**), with EC_{50} decreasing by 17-fold (226 ± 103 pM vs. 13 ± 1.8 pM). LNCaP C4-2B CD46 ADC: LNCaP-C4-2B cells treated with CD46 ADC. LNCaP C4-2B/Abi CD46 ADC: LNCaP-C4-2B cells with prior exposure to abiraterone were treated with CD46 ADC. LNCaP C4-2B Ctrl IgG ADC: LNCaP-C4-2B cells treated with the control ADC (Ctrl IgG-MC-vc-PAB-MMAF). LNCaP C4-2B/Abi Ctrl IgG ADC: LNCaP-C4-2B cells with prior exposure to abiraterone were treated with the control ADC (Ctrl IgG-MC-vc-PAB-MMAF).

in mitotic activity was found in liver, kidney, and spleen, consistent with known drug (auristatin)–induced toxicities. An enlargement of spleen red pulp was observed. Pharmacokinetic analysis was performed, and the half-life of our CD46 ADC was about 4 days (101.4 ± 15.5 hours at 5 mg/kg, $n = 4$).

Discussion

One of the most challenging aspects of cancer therapy development is target selection. Primary tumors often retain tissue differentiation markers that are specific for the tissue from which the tumors are derived. However, these markers are often not functionally required for tumor survival and growth, and as such are often lost as tumor progresses to advanced stages. We hypothesize that there exist another set of tumor cell surface antigens that we term functional antigens that are required for tumor growth, survival, and evasion

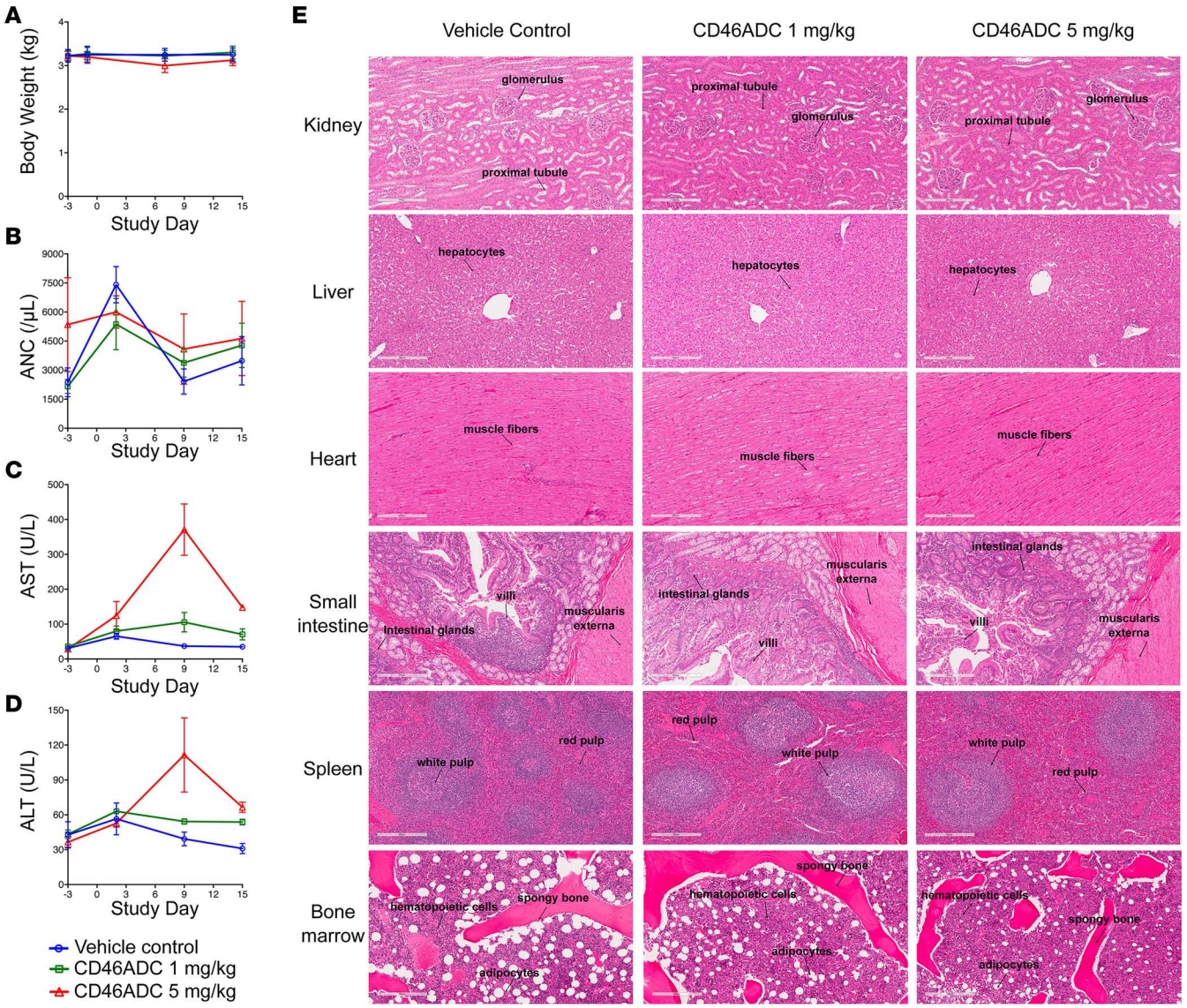

Figure 7. Exploratory tox study in nonhuman primates. (**A**) Cynomolgus monkey body weight (kg) measurement. (**B**) Absolute neutrophil count (ANC; per μl blood). (**C**) AST level. (**D**) ALT level. (**E**) Necropsy analysis. H&E sections of representative male monkeys from each dosing group are shown. Arrows point to tissue substructures as specified. Scale bars: 300 μm.

of the host immune surveillance. These functional antigens are not lost during tumor progression but instead maintained or increased in advanced treatment-resistant tumors, and are thus excellent targets for cancer therapy development. We have previously combined LCM and phage antibody display to select for novel internalizing human mAbs that bind to true tumor antigens expressed by tumor cells in situ as opposed to cell line artifacts. We have identified a lead antibody with desired properties that the above selection scheme was designed to capture. In this study, we identified the target antigen by IP and mass spectrometry analysis as human CD46, a negative regulator of the innate immunity. We showed by IHC that CD46 is highly expressed in both primary and mCRPC specimens. In normal human tissues, CD46 is expressed at low levels except for placental trophoblasts and normal prostate epithelium, and thus has good tissue specificity. Intriguingly, analysis of a public genomic and clinical database as well as the Prostate Cancer West Coast Dream Team internal database showed that the CD46 gene undergoes genomic gain/amplification as the disease progresses from primary to metastatic, and from ASI naive to ASI resistant. CD46 mRNA levels are either maintained at high levels in both adenocarcinoma and neuroendocrine subtypes or trending up as ASI resistance develops. CD46 mRNA and protein are homogenously overexpressed in mCRPC, differentiating it from lineage markers that often shown heterogeneous expression in late-stage cancer.

We found that our anti-CD46 antibody is internalized by receptor-dependent macropinocytosis, an inherently tumor-selective internalization pathway that can confer additional targeting specificity for tumor over normal tissue (34–36, 50). We developed a macropinocytosing CD46 ADC by conjugating the auristatin derivative MMAF to our human monoclonal anti-CD46 antibody and showed potent and selective tumor killing in vitro, not affecting normal cells expressing low levels of CD46. We showed that our CD46 ADC is also potent in vivo against both subcu and intrafemoral mCRPC cell line xenografts. To assess potential toxicity, we performed an exploratory tox study in cynomolgus monkeys and found no overt toxicity at any dose tested (1 and 5 mg/kg) and no evidence of notable on-target toxicity; this was consistent with current understanding of how auristatin-based ADC works, i.e., at clinically relevant doses, toxicity is largely drug dependent and target independent (37). Our study provides a strong rationale for clinical development of CD46 ADC in mCRPC.

It is intriguing but not fully understood why prostate cancer expresses high levels of CD46. It is tempting to hypothesize that tumor cells need to evade the host immune system, innate or adaptive, and CD46 forms part of the defense shield that the tumor uses to evade immune surveillance (51–53). That being said, it is also possible that CD46 performs other functions that are critical for tumor cell invasion, survival, or self-renewal. Regardless of mechanistic details, CD46 is expressed at uniformly high levels as prostate cancer progresses through ASI-resistance and treatment-induced neuroendocrine differentiation, making it a potential novel target for late-stage treatment-resistant form of this disease.

In our IHC study of primary prostate tumor, CD46 signal was rather uniform, and we did not observe a correlation between CD46 staining intensity and tumor grades. The finding is consistent with a previous report (51). As IHC method is not exactly quantitative, more advanced protein measurement methods such as imaging mass spectrometry (54) and single-cell analysis (55) may be used to further investigate this issue.

CD46 is a heavily modified glycoprotein with 4 Sushi domains (27, 56). The Sushi domain is also present in other proteins. Depending on the exact specificity and epitope, anti-CD46 antibodies can generate various IHC staining patterns. For therapeutic development, we emphasized the use of our lead human mAb (YS5, binding to a conformational epitope of CD46) on a frozen human normal tissue array for specificity evaluation by IHC. Our result showed that the YS5 epitope is present on a limited number of normal tissues. Besides normal placental trophoblasts and prostate epithelial cells, the YS5 epitope is either absent or present at low levels on other normal tissues, creating an excellent targeting opportunity. Our exploratory tox study in nonhuman primates also supports the targetability of CD46, as the main tox finding for the ADC is consistent with known drug (MMAF)–related effect that is independent of CD46.

Despite the good tissue specificity, tumor-selective internalization, and lack of notable on-target toxicity in the exploratory tox study in cynomolgus monkeys, one should always consider carefully the potential toxicity of CD46 targeting. CD46 is a multifunctional protein, regulating the complement cascade (56) and pathogen entry into cells (57). It is expressed at low levels on immune cells such as T cells and seems to have diverse regulatory functions (58–61). Targeting CD46 by naked mAb could affect T cell function, although the exact nature of the effect awaits further study, as no anti-CD46 naked mAb has been tested in the clinic. Likewise, targeting CD46 by an ADC could have an effect on T cells, including the possibility of activation-induced internalization and killing of subsets of T cells. The effect of anti-CD46 ADC on the human immune system is expected to be determined from analysis of data generated from future clinical trials.

CD46 mutation is a predisposing but not causative factor for a small fraction (~10%) of atypical hemolytic uremic syndrome, with incomplete penetrance (62). The disease occurs mostly in children (62), a population that is not likely to receive prostate cancer treatment. Most important, our anti-CD46 antibody and ADC bind to a conformational epitope residing in Sushi domains 1 and 2, outside the region that is involved in binding by complement pathway components (63), and thus is unlikely to cause dysregulation of the complement pathway. Indeed, we observed no competition by our anti-CD46 antibody with complement component binding and no enhanced complement activity in vitro. Our exploratory tox study in nonhuman primates also did not detect complement-induced organ damage. As such, our anti-CD46 ADC is not expected to cause excessive terminal complement cascade activation. Conclusive evidence regarding this issue is expected to come from future clinical trials.

Interestingly, CD46 is also a coreceptor for oncolytic measles virus (64) that has already entered into multiple early-phase clinical trials and found to be safe (30, 65, 66). Although ADC is a different class of agent compared with oncolytic measles virus, the excellent safety profile of oncolytic measles virus suggests that CD46 can be targeted in humans without triggering unexpected severe on-target toxicity. Future phase I trials will determine whether CD46 ADC has an acceptable safety profile in mCRPC patients.

Methods

Cell culture. The human mCRPC cell line DU145 and VCaP was obtained from ATCC. The mCRPC line LNCap-C4-2B was originally obtained from UroCor Inc. and maintained in the laboratory. The firefly luciferase–expressing mCRPC line PC3M-luc-C6 (PC3M-luc) was originally obtained from Agilent and maintained in the laboratory. The primary normal human liver cell line HS775li was obtained from the UCSF Cell Culture facility. The benign prostatic hyperplasia epithelial cell line BPH-1 was originally obtained from Gerald Cunha's lab at UCSF and maintained in the laboratory. A normal human primary prostate epithelial cell line (HPrEpC) was purchased from Cell Applications Inc. and cultured in the epithelial cell growth medium provided by the vendor. A normal cynomolgus prostate epithelial cell line was purchased from Cell Biologics Inc. and cultured in the epithelial cell growth medium provided by the vendor. Human $CD3^+$ T cells and CD14-depleted peripheral blood mononuclear cells (PBMCs) (Astarte) were maintained in RPMI-1640 supplemented with 10% FBS. The NEPC cell line H660 obtained from ATCC was cultured in RPMI 1640 supplemented with 0.005 mg/ml insulin, 0.01 mg/ml transferrin, 30 nM sodium selenite, 10 nM hydrocortisone, 10 nM β-estradiol, 4 mM L-glutamine, and 5% FBS. Unless specified, all other cell lines were maintained in DMEM supplemented with 10% FBS (Thermo Fisher Scientific) and 100 μg/ml penicillin-streptomycin. All cell lines were cultured in a humidified atmosphere of 95% air and 5% CO_2 at 37°C.

Recombinant Fc-fusion protein. The UA20 scFv and CD46 extracellular Sushi domains 1 and 2 were subcloned into the Fc fusion expression vector pFUSE-hIgG1 Fc2 (InvivoGen) and transfected into HEK293a cells by Lipofectamine 2000 (Thermo Fisher Scientific, Life Technologies). Supernatants were collected, filtered by 0.22-μm filter (Millipore), and purified on protein A beads (Thermo Fisher Scientific, Pierce).

Ectopic expression of the CD46 gene. Genes encoding human and cynomolgus CD46, and hemagglutinin from the Edmonston strain measles virus, were synthesized (GenScript) and subcloned into pCI-neo mammalian expression vector (OriGene). Mammalian cells (CHO-K1 or HEK293) were transfected with human and cynomolgus monkey CD46 expression constructs using Lipofectamine 2000 (Life Technologies). FACS analysis was performed using anti-CD46 antibodies (YS5 or others as indicated in the text), followed by detection with Alexa Fluor 647–conjugated goat anti-human secondary antibody (Jackson ImmunoResearch Laboratories Inc.).

A panel of human monoclonal anti-CD46 antibodies. Both phage display and yeast display were used to identify human mAbs binding to CD46 using methods that we have described (31, 32). Recombinant CD46 (domains 1+2)–Fc was used as the bait to select binders from a non-immune phage display library (32) and in parallel from a yeast display library generated by transfer of a phage library enriched for tumor cell surface binders (31). Positive clones were sequenced, and unique scFvs were converted to full-length human IgG1 using methods described previously (21, 67). The expression vector was modified from the Abvec vector that was originally provided by Patrick Wilson (University of Chicago, Chicago, Illinois, USA) (67). The antibodies were transiently expressed in HEK293A cells following polyethylenimine (Sigma-Aldrich) transfection. The secreted antibody in serum-free DMEM containing Nutridoma-SP (Roche) and penicillin-streptomycin were harvested after 5 days of incubation and purified using protein A agarose (Thermo Fisher Scientific, Pierce). Antibody concentrations were determined using Nanodrop 2000 (Thermo Fisher Scientific).

IP and mass spectrometry analysis. DU145 and BPH-1 cells were biotin-labeled with EZ-Link Sulfo-NHS-LC-Biotinylation Kit (Thermo Fisher Scientific, Pierce) and lysed with cell lysis buffer (20 mM Tris-HCl, pH 7.4, 0.3 M NaCl, 1% Nonidet P-40) supplemented with complete protease inhibitor cocktail (Roche). The UA20 scFv–Fc fusion molecule was conjugated to protein G agarose beads (Sigma-Aldrich) in 20 mM dimethyl pimelimidate dihydrochloride (DMP) to bring the final concentration to 20 mM, pH 8.3, at room temperature (RT) for 30 minutes, washed once with ethanolamine (0.2 M, pH 8.0), and further incubated with ethanolamine (0.2 M, pH 8.0) for 4 hours at RT to terminate the reaction. The antibody-conjugated beads were incubated with cell lysates at 4°C overnight, washed 3 times with cell lysis buffer and 3 times with PBS, boiled in SDS-PAGE sample buffer, and loaded onto a SDS-PAGE gradient gel (10%–20%) (Thermo Fisher Scientific, Invitrogen) in duplicate, one for silver staining (Thermo Fisher Scientific, Pierce) and the other for Western blot analysis to locate the membrane protein bands using HRP-conjugated streptavidin (Jackson ImmunoResearch Laboratories Inc.) and ECL substrate (Thermo Fisher Scientific, Pierce). Silver-stained bands corresponding to positions on the Western blot were excised, in-gel digested with trypsin, and analyzed on Q-Star Elite mass spectrometer (AB Sciex; at UCSF Mass Spectrometry Facility). Spectra were searched using Protein Prospector against the SwissProt database (https://www.uniprot.org/).

Flow cytometry. Cell binding and apparent K_D measurement by FACS was performed as described previously (20, 21, 68), using appropriate secondary antibodies on a BD Accuri cC6 (BD Biosciences). Median fluorescence intensity (MFI) was used for curve fitting using Prism 6.0 (GraphPad) to give the estimated apparent K_D value.

Binding domain determination by deletion mapping. Plasmids expressing CD46 deletion mutants were transiently transfected into HEK293 cells. Anti-CD46 antibody binding was determined by FACS and expressed as percentage of binding to full-length WT CD46.

Immunofluorescence confocal microscopy. DU145, LNCaP-C4-2B, and PC3M-luc cells (5,000 per well) were grown overnight in glass chamber slides (Thermo Fisher Scientific, Lab-Tek) at 37°C, incubated with 20 μg/ml YS5 IgG1 for the indicated time periods (4 and 24 hours) with Texas red–conjugated 70-kDa neutral dextran ND70-TR (a macropinocytosis marker; Thermal Fisher Scientific, Life Technologies), washed with PBS, fixed with 4% paraformaldehyde (PFA), and permeabilized with PBS containing 0.1% Triton X-100 and 1% BSA. The YS5 IgG1 was identified with Alexa Fluor 647–conjugated goat anti-human antibody (Jackson ImmunoResearch Laboratories Inc.). Nuclei were identified by counterstaining cells with Hoechst (Thermo Fisher Scientific, Life Technologies). Subcellular structures were marked by polyclonal rabbit antibodies against LAMP-1 (lysosomal marker), followed by detection with FITC-labeled donkey anti-rabbit antibody (Jackson ImmunoResearch Laboratories Inc.). Staining was analyzed with a fully automated FluoView confocal microscope (Olympus) (21).

IHC. Frozen tissue array sections were fixed in cold acetone by the vendor (US Biomax). They were air-dried for 20 minutes at RT, fixed in 4% PFA for 15 minutes per the vendor's recommendation, washed 3 times with PBS, incubated with 3% H_2O_2 (Invitrogen) for 10 minutes to block endogenous peroxidase activity, further blocked with 2% goat serum and avidin/biotin (Vector Laboratories), washed 3 times with PBS, incubated with 10 μg/ml biotinylated YS5 IgG1 at 4°C overnight, and washed 3 times with PBS, with bound antibody detected by streptavidin-HRP (catalog 016-030-084, Jackson ImmunoResearch Laboratories Inc.) using diaminobenzidine as substrate (Agilent, Dako). The biotinylated nonbinding human IgG1 YSC10 was used for negative control. Placenta was used for positive control and heart for negative control.

Paraffin tissue array sections (US Biomax) were deparaffinized in xylene (Sigma-Aldrich) overnight; rehydrated by sequential incubation in 100%, 95%, and 70% ethanol; and treated with unmasking solution (Vector Laboratories) according to manufacturer's instructions. Following sequential blocking with 3% H_2O_2, 2% donkey serum (Santa Cruz Biotechnology Inc.) and avidin/biotin as described above, the tissue array slides were incubated with rabbit anti-CD46 affinity-purified polyclonal antibody H-294 (catalog sc-9098, Santa Cruz Biotechnology Inc., 1:400 dilution) at 4°C overnight, washed 3 times with PBS, and further incubated with Dako EnVision+ anti-rabbit polymer system (Dako). Rabbit serum was used as negative control. Slides were counterstained with hematoxylin (Sigma-Aldrich); dehydrated by sequential incubation in 70%, 95%, 100% ethanol, and xylene; mounted in VectaMount (Vector Laboratories); and observed by BZ-9000 digital microscopy (Keyence).

IHC results were evaluated by a semiquantitative approach using H-score using the following formula: 1 × (% cells 1+) + 2 × (% cells 2+) + 3 × (% cells 3+), as described previously (69). Staining intensity was graded as 0, 1+, 2+, or 3+ for each cell in a fixed field.

Immunotoxin assay. The assay was performed as described previously (21). Briefly, DU145, C4-2B, HS775li, and BPH-1 cells were seeded at 1,000 cells/well in a 96-well plate (Falcon) and cultured at 37°C overnight. Biotinylated UA20 IgG and Streptavidin-ZAP (SA-ZAP; Advanced Targeting Systems) were mixed at a molar ratio of 1:1 on ice for 30 minutes to form the CD46-targeted immunotoxin. Cells were incubated with various amounts of immunotoxin (final concentration of SA-ZAP was 0, 0.6, 6, 60, and 300 nM) at 37°C for 96 hours. Live cell number was determined using a CCK-8 assay following the manufacturer's instruction (Dojindo).

Complement element competition assay. Du-145 cells were fixed by 2% PFA, washed and resuspended in PBS, and incubated with anti-CD46 antibodies at 20 μg/ml for 1 hour at RT. Purified human C3b (Complement Technology Inc.) were added at 100 μg/ml at RT for an additional 1 hour. No human serum or any other complement components were used during incubation. Cells were washed with PBS, incubated with mouse anti-C3b antibody (Thermo Fisher Scientific/Pierce) at RT for 1 hour, washed with PBS, and incubated with Alexa Fluor 647–conjugated goat anti-mouse antibody (Jackson ImmunoResearch Laboratories Inc.) to detect cell-bound CD3b by FACS.

H protein competition assay. Potential competition between oncolytic measles virus hemagglutinin and our CD46 mAbs was determined by FACS. All binding reactions were performed in 0.05% NaN_3 to prevent endocytosis. DU145 cells were incubated with unlabeled anti-CD46 antibodies at 20 μg/ml for 1 hour at RT, then biotin-labeled soluble H protein–Fc fusion (sH-Fc) at a concentration of 100 μg/ml for 1 hour at RT, followed by incubation with Alexa Fluor 647–conjugated streptavidin (Jackson ImmunoResearch Laboratories Inc.) for 30 minutes at RT to detect bound sH-Fc. The percentage of inhibition was calculated from MFI values using the following formula: $(MFI_{\text{sH binding without mAb}} - MFI_{\text{sH binding with mAb}}) \times 100/MFI_{\text{sH binding without mAb}}$.

Creation and analysis of CD46 ADC. ADC creation was described previously by us (50). Briefly, YS5 (aka 23AG2) IgG1 was resuspended in 100 nM phosphate with 150 nM NaCl (pH 8.0) and was partially reduced with 2 equivalents of Tris(2-carboxyethyl) phosphine hydrochloride (TCEP) at 37°C for 2 hours. The mixture was purified by Zeba spin column (Thermo Fisher Scientific, Pierce) and buffer-exchanged into PBS with 5 mM EDTA. Six equivalents of maleimidocaproyl valine-citrulline monomethyl auristatin phenylalanine (MC-vc-PAB-MMAF) was incubated with TCEP-reduced antibodies at RT for 1 hour. Excess MC-vc-PAB-MMAF was removed by running twice through the Zeba spin column. Purified ADCs were analyzed by hydrophobic interaction chromatography (HIC)-HPLC with infinity 1220 LC System (Agilent). The drug-to-antibody ratio was estimated from area integration using OpenLab CDS software (Agilent).

In vitro ADC cytotoxicity assay. DU145, LNCaP-C4-2B, PC3M-luc, BPH-1, and $CD3^+$ T cells and CD14-depleted PBMCs were placed into 96-well plates at 2,000 cell/well and incubated with serially diluted ADCs at indicated concentrations for 96 hours at 37°C in a humidified chamber with 5% CO_2. The media was removed, and cells were gently washed once with PBS. Calcein AM (1 μM) (Invitrogen) in PBS was added, and cells were incubated for 40 minutes at RT. Plates were then read on a fluorescence plate reader (BioTek) using an excitation wavelength of 485 nm and an emission wavelength of 530 nm. Percent cell survival was normalized against mock-treated cells. EC_{50} was determined by Prism 6.0 (GraphPad).

In vivo subcu xenograft study. All animal studies were approved by the UCSF Animal Care and Use Committee (AN092211) and conducted in adherence to the NIH *Guide for the Care and Use of Laboratory Animals* (National Academies Press, 2011). Mouse number per study group was determined according to a previous study with CD46 ADC (50) and other ADCs published in the literature (70) rather than power calculation. Male nude mice (Ncr nude, sp/sp, Taconic) at 7–9 weeks of age were implanted with 1×10^6 LNCaP-C4-2B cells in 100 μl PBS subcu at the flank of the animal. Growing tumors were palpated, and sizes measured by a caliper. Tumor volume was calculated using the formula $V = ½ (\text{length} \times \text{width}^2)$. When the tumor reached a volume of ~400–500 mm^3, the animals were randomized into 5 groups and dosed i.v. with 5 mg/kg YS5 ADC and control ADC/agents for a total of 4 doses on days 21, 24, 28, and 34 after subcu grafting. Body weight and other signs of overt toxicity were monitored daily.

Evaluation of ADC in intrafemoral xenograft model. NSG (NOD.Cg-*Prkdc*^{scid} *Il2rg*^{tm1Wjl}/SzJ, 5 male, 5 female, The Jackson Laboratory) mice at 10–12 weeks of age were intrafemorally injected with the 5×10^4 LNCaP-C4-2B-luc line, which was engineered by lentiviral transduction to expresses the firefly luciferase gene. The YS5 ADC or control ADC was injected 7 days after tumor grafting at 4 mg/kg, every 4 days for a total of 4 doses. Tumor status was monitored by bioluminescence imaging. Briefly, 0.2 ml of 10 mg/ml luciferin solution was injected i.v. into each mouse via the tail vein under anesthesia. The photon emitted was immediately measured (Xenogen IVIS). Images were analyzed using Igor Pro Carbon/Living Image (WaveMetrics). Body weight and other signs of overt toxicity were monitored daily.

CTC enrichment and analysis. CTCs from mCRPC patient blood samples (20 ml) were enriched using the cell adhesion matrix (CAM) + FACS assay described previously (71). Briefly, blood from patients was incubated with RBC lysis buffer in a 50-ml conical tube for 5 minutes. Nucleated cells were pelleted by centrifugation, resuspended, added to a Vita-Assay (fluorescent green CAM-coated) plate (Vitatex), and incubated at 37°C with RBC lysis buffer in a 50-ml conical tube for 5 minutes. Nucleated cells were released from the plates using Cell Releasing CAM Enzyme (Vitatex). Cells were concentrated and analyzed on an Aria III (BD Biosciences) flow cytometer. Annexin V–Pacific blue (Thermo Fisher Scientific) staining was used as the live/dead cell marker according to the manufacturer's recommendations. Enriched cells from the CAM assay were stained with biotin-labeled anti-CD46 mAb followed by R-phycoerythrin–conjugated streptavidin (1:1,000) and allophycocyanin-conjugated anti-CD45/CD14 (1:33) antibodies. The YSC10 IgG1 was used as an isotype control. CTCs that were positive for CD46 were identified by annexin^{lo}, CAM^{hi}, CD46^{hi}, and CD45/14^{lo}. The FACS data was analyzed with FlowJo (Tree Star Inc.).

Cell surface antigen copy number determination. Antigen density was determined by quantitative FACS as we have described previously (50). Briefly, anti-CD46 antibody, anti-PSMA antibody, and nonbinding control antibody were directly conjugated to Alexa Fluor 647 fluorescence using an Alexa Fluor 647 Monoclonal Antibody Labeling Kit (Thermo Fisher Scientific, Invitrogen) following the manufacturer's instructions. Binding of Alexa Fluor 647–labeled mAb to cells was detected by FACS. The effective fluorophore/protein (F/P) ratio of the labeled antibody was determined by Simply Cellular anti-Human IgG. MFI was converted to molecules of equivalent soluble fluorochrome (MESF) using a standard curve generated by Quantum beads using quantitative analysis template QuickCal v.2.3 software (Bangs Laboratories). MESF was converted to Antibody Binding Capacity (ABC) by determining the F/P ratio.

Coculture in condition media from bone marrow/stroma cells. Human bone marrow/stroma cell line HS-5 was cultured in DMEM medium supplemented with 10% FBS. Supernatant were collected every 4 days, filtered with a 0.22 μM vacuum filter cup (EMD), and stored at –80°C until use in experiments. LNCaP-C4-2B, DU145, and PC3M-luc cells were cultured in 24-well plates to 80% confluence, washed with PBS, and incubated with fresh medium containing 50% HS-5 condition medium and 50% DMEM/10% FCS for 3–7 days (47). Cell surface copy number of CD46 and PSMA was determined by quantitative FACS. Neuroendocrine feature was assessed by anti-NSE antibody (Dako) by Western blot.

Exploratory tox study in nonhuman primate. The tox study was performed at the Toxicology Division of WuXi AppTec (Suzhou) Co. Twelve cynomolgus monkeys (~3 years of age, 2.9–3.8 kg) were assigned to 3 treatment groups: vehicle control, YS5 ADC at 1 and 5 mg/kg. For each group, 4 animals per dosage group were used, 2 male and 2 female. A single bolus i.v. injection was given on day 1. The animals were evaluated for changes in body weight, mortality, food consumption, and pathology indices. Blood samples were collected for hematology, blood chemistry, and pharmacokinetic studies. Necropsy was performed on day 15. Tissues were fixed in 10% formalin and processed for paraffin embedding. Sections were cut and stained with hematoxylin and eosin, and examined under a microscope by a resident pathologist.

Statistics. Statistical analysis was done using GraphPad Prism v6.0. Two-tailed Student's *t* test was used when comparing 2 group means. One-way ANOVA was used for comparing means of 3 or more groups. *P* values less than 0.05 were considered significant, and are indicated in the figures as $*P < 0.05$, $**P < 0.01$, $***P < 0.001$, and $****P < 0.0001$.

Study approval. Archived prostate cancer tissues were analyzed. They were collected in a separate study (8) by the West Coast Prostate Cancer Dream Team with institutional approval. Written informed consent was obtained from all individuals who donated samples. Identifying patient information was replaced with sequentially assigned numbers, in accordance with Health Insurance Portability and Accountability Act (HIPAA) guidelines. Mouse studies were approved by the UCSF Animal Care and Use Committee (AN142193-02).

Author contributions

Y. Su designed and executed experiments, collected, analyzed and interpreted data, and wrote the manuscript. YL, CRB, and SB designed and executed experiments, collected, analyzed and interpreted data, and wrote sections of the manuscript. NKL performed experiments and collected and analyzed data. RA, a urologic oncologist, collected, analyzed, and interpreted clinical data. DWS, ALB, and BCH designed and executed experiments, and collected, analyzed, and interpreted data. JPS, a pathologist, analyzed and interpreted IHC data. GP and PLP designed and executed experiments and collected, analyzed, and interpreted data. MAS, a medical oncologist, analyzed data and provided clinical input and interpretation. Y. Seo performed experiments and collected and analyzed data. EJS, a medical oncologist, collected, and analyzed data and provided clinical input and interpretation. BL conceived the overall project idea, designed experiments, analyzed and interpreted data, and wrote the manuscript. All authors critically reviewed the manuscript.

Acknowledgments

We thank Zhaogang Dong and Xin Zhang for help with experiments during the early phase of the project; Kathy Li for help with mass spectrometry analysis; and Donghui Wang, Paul Phojanakong, Julia Malato, and Fernando Salangsang at the Experimental Therapeutic Core for help with in vivo studies. The work is supported by grants from the NIH/National Cancer Institute (R01 CA118919, R01 CA171315, and R01 CA129491 to BL); UCSF prostate cancer program development project fund (to BL); Stand Up To Cancer–Prostate Cancer Foundation (SU2C-PCF2) Dream Team (to EJS); Biomedical Technology Research

Centers program of the NIH National Institute of General Medical Sciences (8P41GM103481 to ALB); and the Dr. Miriam and Sheldon G. Adelson Medical Research Foundation (to ALB).

Address correspondence to: Bin Liu, Department of Anesthesia/UCSF, 1001 Potrero Avenue, 1305, San Francisco, California 94143, USA. Phone: 415.206.6073; Email: bin.liu@ucsf.edu.

1. Ryan CJ, Molina A, Griffin T. Abiraterone in metastatic prostate cancer. *N Engl J Med*. 2013;368(15):1458–1459.
2. Ryan CJ, et al. Abiraterone in metastatic prostate cancer without previous chemotherapy. *N Engl J Med*. 2013;368(2):138–148.
3. Ryan CJ, Cheng ML. Abiraterone acetate for the treatment of prostate cancer. *Expert Opin Pharmacother*. 2013;14(1):91–96.
4. Ryan CJ, et al. Targeted MET inhibition in castration-resistant prostate cancer: a randomized phase II study and biomarker analysis with rilotumumab plus mitoxantrone and prednisone. *Clin Cancer Res*. 2013;19(1):215–224.
5. Loriot Y, et al. Antitumour activity of abiraterone acetate against metastatic castration-resistant prostate cancer progressing after docetaxel and enzalutamide (MDV3100). *Ann Oncol*. 2013;24(7):1807–1812.
6. Loriot Y, Fizazi K. Taxanes: still a major weapon in the armamentarium against prostate cancer. *Eur Urol*. 2013;63(6):983–985.
7. Beltran H, et al. Divergent clonal evolution of castration-resistant neuroendocrine prostate cancer. *Nat Med*. 2016;22(3):298–305.
8. Aggarwal R, et al. Clinical and genomic characterization of treatment-emergent small-cell neuroendocrine prostate cancer: a multi-institutional prospective study. *J Clin Oncol*. 2018;36(24):2492–2503.
9. Carter PJ, Lazar GA. Next generation antibody drugs: pursuit of the 'high-hanging fruit'. *Nat Rev Drug Discov*. 2018;17(3):197–223.
10. Pastan I, Hassan R. Discovery of mesothelin and exploiting it as a target for immunotherapy. *Cancer Res*. 2014;74(11):2907–2912.
11. Chang K, Pastan I. Molecular cloning of mesothelin, a differentiation antigen present on mesothelium, mesotheliomas, and ovarian cancers. *Proc Natl Acad Sci USA*. 1996;93(1):136–140.
12. Reiter RE, et al. Prostate stem cell antigen: a cell surface marker overexpressed in prostate cancer. *Proc Natl Acad Sci USA*. 1998;95(4):1735–1740.
13. Gualberto A. Brentuximab Vedotin (SGN-35), an antibody-drug conjugate for the treatment of CD30-positive malignancies. *Expert Opin Investig Drugs*. 2012;21(2):205–216.
14. Li D, et al. DCDT2980S, an anti-CD22-monomethyl auristatin E antibody-drug conjugate, is a potential treatment for non-Hodgkin lymphoma. *Mol Cancer Ther*. 2013;12(7):1255–1265.
15. Boswell CA, et al. Impact of drug conjugation on pharmacokinetics and tissue distribution of anti-STEAP1 antibody-drug conjugates in rats. *Bioconjug Chem*. 2011;22(10):1994–2004.
16. Silver DA, Pellicer I, Fair WR, Heston WD, Cordon-Cardo C. Prostate-specific membrane antigen expression in normal and malignant human tissues. *Clin Cancer Res*. 1997;3(1):81–85.
17. Lin JC, et al. TROP2 is epigenetically inactivated and modulates IGF-1R signalling in lung adenocarcinoma. *EMBO Mol Med*. 2012;4(6):472–485.
18. Kristiansen G, et al. ALCAM/CD166 is up-regulated in low-grade prostate cancer and progressively lost in high-grade lesions. *Prostate*. 2003;54(1):34–43.
19. Liu B, Conrad F, Cooperberg MR, Kirpotin DB, Marks JD. Mapping tumor epitope space by direct selection of single-chain Fv antibody libraries on prostate cancer cells. *Cancer Res*. 2004;64(2):704–710.
20. An F, et al. Targeted drug delivery to mesothelioma cells using functionally selected internalizing human single-chain antibodies. *Mol Cancer Ther*. 2008;7(3):569–578.
21. Ha KD, Bidlingmaier SM, Zhang Y, Su Y, Liu B. High-content analysis of antibody phage-display library selection outputs identifies tumor selective macropinocytosis-dependent rapidly internalizing antibodies. *Mol Cell Proteomics*. 2014;13(12):3320–3331.
22. Becerril B, Poul MA, Marks JD. Toward selection of internalizing antibodies from phage libraries. *Biochem Biophys Res Commun*. 1999;255(2):386–393.
23. Ha KD, Bidlingmaier SM, Su Y, Lee NK, Liu B. Identification of novel macropinocytosing human antibodies by phage display and high-content analysis. *Meth Enzymol*. 2017;585:91–110.
24. Ruan W, Sassoon A, An F, Simko JP, Liu B. Identification of clinically significant tumor antigens by selecting phage antibody library on tumor cells in situ using laser capture microdissection. *Mol Cell Proteomics*. 2006;5(12):2364–2373.
25. Su Y, Bidlingmaier S, Lee NK, Liu B. Combine phage antibody display library selection on patient tissue specimens with laser capture microdissection to identify novel human antibodies targeting clinically relevant tumor antigens. *Methods Mol Biol*. 2018;1701:331–347.
26. He J, et al. Targeting prostate cancer cells in vivo using a rapidly internalizing novel human single-chain antibody fragment. *J Nucl Med*. 2010;51(3):427–432.
27. Seya T, Turner JR, Atkinson JP. Purification and characterization of a membrane protein (gp45-70) that is a cofactor for cleavage of C3b and C4b. *J Exp Med*. 1986;163(4):837–855.
28. Stirpe F, Barbieri L, Battelli MG, Soria M, Lappi DA. Ribosome-inactivating proteins from plants: present status and future prospects. *Biotechnology (NY)*. 1992;10(4):405–412.
29. Vago R, et al. Saporin and ricin A chain follow different intracellular routes to enter the cytosol of intoxicated cells. *FEBS J*. 2005;272(19):4983–4995.
30. Galanis E, et al. Phase I trial of intraperitoneal administration of an oncolytic measles virus strain engineered to express carcinoembryonic antigen for recurrent ovarian cancer. *Cancer Res*. 2010;70(3):875–882.
31. Bidlingmaier S, Su Y, Liu B. Combining phage and yeast cell surface antibody display to identify novel cell type-selective internalizing human monoclonal antibodies. *Methods Mol Biol*. 2015;1319:51–63.
32. Lee NK, Bidlingmaier S, Su Y, Liu B. Modular construction of large non-immune human antibody phage-display libraries from variable heavy and light chain gene cassettes. *Methods Mol Biol*. 2018;1701:61–82.
33. Crimeen-Irwin B, et al. Ligand binding determines whether CD46 is internalized by clathrin-coated pits or macropinocytosis. *J Biol Chem*. 2003;278(47):46927–46937.

34. Commisso C, et al. Macropinocytosis of protein is an amino acid supply route in Ras-transformed cells. *Nature*. 2013;497(7451):633–637.
35. Ha KD, Bidlingmaier SM, Liu B. Macropinocytosis exploitation by cancers and cancer therapeutics. *Front Physiol*. 2016;7:381.
36. Reyes-Reyes EM, Teng Y, Bates PJ. A new paradigm for aptamer therapeutic AS1411 action: uptake by macropinocytosis and its stimulation by a nucleolin-dependent mechanism. *Cancer Res*. 2010;70(21):8617–8629.
37. de Goeij BE, Lambert JM. New developments for antibody-drug conjugate-based therapeutic approaches. *Curr Opin Immunol*. 2016;40:14–23.
38. Gao J, et al. Integrative analysis of complex cancer genomics and clinical profiles using the cBioPortal. *Sci Signal*. 2013;6(269):pl1.
39. Cerami E, et al. The cBio cancer genomics portal: an open platform for exploring multidimensional cancer genomics data. *Cancer Discov*. 2012;2(5):401–404.
40. Kumar A, et al. Substantial interindividual and limited intraindividual genomic diversity among tumors from men with metastatic prostate cancer. *Nat Med*. 2016;22(4):369–378.
41. Robinson D, et al. Integrative clinical genomics of advanced prostate cancer. *Cell*. 2015;161(5):1215–1228.
42. Grasso CS, et al. The mutational landscape of lethal castration-resistant prostate cancer. *Nature*. 2012;487(7406):239–243.
43. Cancer Genome Atlas Research Network. The molecular taxonomy of primary prostate cancer. *Cell*. 2015;163(4):1011–1025.
44. Gao D, et al. Organoid cultures derived from patients with advanced prostate cancer. *Cell*. 2014;159(1):176–187.
45. Baca SC, et al. Punctuated evolution of prostate cancer genomes. *Cell*. 2013;153(3):666–677.
46. Aggarwal R, et al. Targeting Adaptive pathways in metastatic treatment-resistant prostate cancer: update on the Stand Up 2 Cancer/Prostate Cancer Foundation–supported West Coast Prostate Cancer Dream Team. *Eur Urol Focus*. 2016;2(5):469–471.
47. Spiotto MT, Chung TD. STAT3 mediates IL-6-induced growth inhibition in the human prostate cancer cell line LNCaP. *Prostate*. 2000;42(2):88–98.
48. Mertz KD, et al. Molecular characterization of TMPRSS2-ERG gene fusion in the NCI-H660 prostate cancer cell line: a new perspective for an old model. *Neoplasia*. 2007;9(3):200–206.
49. Leipold D, Mallet WG. Case study: an antibody–drug conjugate targeting muc16 for ovarian cancer. In: Phillips G, ed. *Antibody-Drug Conjugates and Immunotoxins Cancer Drug Discovery and Development*. New York, New York, USA: Springer; 2013:221–239.
50. Sherbenou DW, et al. Antibody-drug conjugate targeting CD46 eliminates multiple myeloma cells. *J Clin Invest*. 2016;126(12):4640–4653.
51. Loberg RD, Wojno KJ, Day LL, Pienta KJ. Analysis of membrane-bound complement regulatory proteins in prostate cancer. *Urology*. 2005;66(6):1321–1326.
52. Surowiak P, et al. CD46 expression is indicative of shorter revival-free survival for ovarian cancer patients. *Anticancer Res*. 2006;26(6C):4943–4948.
53. Maciejczyk A, et al. CD46 Expression is an unfavorable prognostic factor in breast cancer cases. *Appl Immunohistochem Mol Morphol*. 2011;19(6):540–546.
54. Chaurand P, Schwartz SA, Billheimer D, Xu BJ, Crecelius A, Caprioli RM. Integrating histology and imaging mass spectrometry. *Anal Chem*. 2004;76(4):1145–1155.
55. Bjornson ZB, Nolan GP, Fantl WJ. Single-cell mass cytometry for analysis of immune system functional states. *Curr Opin Immunol*. 2013;25(4):484–494.
56. Liszewski MK, Post TW, Atkinson JP. Membrane cofactor protein (MCP or CD46): newest member of the regulators of complement activation gene cluster. *Annu Rev Immunol*. 1991;9:431–455.
57. Cattaneo R. Four viruses, two bacteria, and one receptor: membrane cofactor protein (CD46) as pathogens' magnet. *J Virol*. 2004;78(9):4385–4388.
58. Le Friec G, et al. The CD46-Jagged1 interaction is critical for human TH1 immunity. *Nat Immunol*. 2012;13(12):1213–1221.
59. Kemper C, Chan AC, Green JM, Brett KA, Murphy KM, Atkinson JP. Activation of human CD4+ cells with CD3 and CD46 induces a T-regulatory cell 1 phenotype. *Nature*. 2003;421(6921):388–392.
60. Sánchez A, Feito MJ, Rojo JM. CD46-mediated costimulation induces a Th1-biased response and enhances early TCR/CD3 signaling in human CD4+ T lymphocytes. *Eur J Immunol*. 2004;34(9):2439–2448.
61. Cardone J, et al. Complement regulator CD46 temporally regulates cytokine production by conventional and unconventional T cells. *Nat Immunol*. 2010;11(9):862–871.
62. Fremeaux-Bacchi V, et al. Genetic and functional analyses of membrane cofactor protein (CD46) mutations in atypical hemolytic uremic syndrome. *J Am Soc Nephrol*. 2006;17(7):2017–2025.
63. Forneris F, et al. Regulators of complement activity mediate inhibitory mechanisms through a common C3b-binding mode. *EMBO J*. 2016;35(10):1133–1149.
64. Dörig RE, Marcil A, Chopra A, Richardson CD. The human CD46 molecule is a receptor for measles virus (Edmonston strain). *Cell*. 1993;75(2):295–305.
65. Msaouel P, et al. Clinical trials with oncolytic measles virus: current status and future prospects. *Curr Cancer Drug Targets*. 2018;18(2):177–187.
66. Russell SJ, et al. Remission of disseminated cancer after systemic oncolytic virotherapy. *Mayo Clin Proc*. 2014;89(7):926–933.
67. Smith K, et al. Rapid generation of fully human monoclonal antibodies specific to a vaccinating antigen. *Nat Protoc*. 2009;4(3):372–384.
68. Liu B, Conrad F, Roth A, Drummond DC, Simko JP, Marks JD. Recombinant full-length human IgG1s targeting hormone-refractory prostate cancer. *J Mol Med*. 2007;85(10):1113–1123.
69. Hirsch FR, et al. Epidermal growth factor receptor in non-small-cell lung carcinomas: correlation between gene copy number and protein expression and impact on prognosis. *J Clin Oncol*. 2003;21(20):3798–3807.
70. Tai YT, et al. Novel anti-B-cell maturation antigen antibody-drug conjugate (GSK2857916) selectively induces killing of multiple myeloma. *Blood*. 2014;123(20):3128–3138.
71. Premasekharan G, et al. An improved CTC isolation scheme for pairing with downstream genomics: demonstrating clinical utility in metastatic prostate, lung and pancreatic cancer. *Cancer Lett*. 2016;380(1):144–152.